

**Component Specific Luminescence of Natural
Minerals and their Application to the Dosimetry of
Natural Radiation Environment**

A THESIS

Submitted for the Award of Ph. D degree of

MOHANLAL SUKHADIA UNIVERSITY

in the

Faculty of Science

by

Madhav Krishna Murari



Under the Supervision of

**K. P. Subramanian, Associate Professor,
Physical Research Laboratory, Ahmedabad**

DEPARTMENT OF PHYSICS

FACULTY OF SCIENCE

MOHANLAL SUKHADIA UNIVERSITY

UDAIPUR

Year of submission: 200

CERTIFICATE

I feel great pleasure in certifying that the thesis entitled Component specific luminescence of natural minerals and their application to the dosimetry of natural radiation environment embodies a record of the results of investigations carried out by Mr. Madhav Krishna Murari under my guidance. I am satisfied with the analysis of data, interpretation of results and conclusions drawn.

He has completed the residential requirement as per rules.

I recommend the submission of thesis.

DECLARATION

I hereby declare that the work incorporated in the present thesis entitled “Component specific luminescence of natural minerals and their application to the dosimetry of natural radiation environment” is my own work and is original. This work (in part or in full) has not been submitted to any University for the award of a Degree or a Diploma.

Signature of the Candidate

Acknowledgement

I sincerely thank Prof. K. P. Subramanian under whom I am registered as a Ph. D. student. His timely help and interest in my research has greatly benefited me. I am deeply indebted to my supervisor Prof. A. K. Singhvi whose guidance and efforts made this project possible. His penchant for perfection has been a continuous source of inspiration to do the best. I have greatly benefited from his experimental acumen and vast knowledge of the physics. In the same spirit I thank Dr. Navin Juyal who was always present when I needed him badly. I am also thankful to Mr. Pranav Adhyaru for all his support.

The company of Prof. M. D. Sastry gave me an opportunity to educate myself in finer aspects of the field of spectroscopy. I express my gratitude for all concern he has shown for my development. I also express my gratitude to Dr. K. P. N. Murthy who introduced me to Monte-Carlo methods at IGCAR. His enthusiasm and energetic nature has greatly inspired me.

I am thankful to all the lab members Yogesh, Mortheikai, Anil, Dattatray, Rabiul and Naveen for providing a friendly and dynamic environment. I greatly appreciate their readiness to help irrespective of situation. I am also grateful to Manoj Tomar who introduced me to MATLAB, fantastic software that contributed to my research.

Finally, I am grateful to *Physical Research Laboratory* for all its support and

Abstract

The thesis explores the fine features of optically stimulated luminescence (OSL) decay and examines the implication of the use of the components in dating and radiation dosimetric applications. This analysis is based on the premise that OSL decay comprises several components arising from various traps with different photo-ionization cross sections. The component interpretation of luminescence has profound implication as regards to the environmental dosimetry and its usage to establish the chronology of various geological events like sediment transport and deposition.

A key aspect of environmental luminescence dosimetry is to ascertain that the luminescence was zero or near zero at the time of deposition of sediments. Determination of true dose or paleodose is needed for all applications. For sediments, the zeroing occurs via photo-bleaching by natural daylight during the transport of sediment. A complete resetting of the signal depends on factors such as spectrum and flux of daylight seen by minerals constituting the sediments. In general, barring a few exceptions, grains in a sediment matrix are partially and heterogeneously bleached. Consequently there is a residual dose distribution which leads to erroneous estimation of age. This thesis examines the prospects of easily bleached OSL components for determining true paleodose acquired by sample.

Isolation of OSL components and their validation forms a major part of this thesis. Numerical experiments on synthetic OSL profiles with superposition of Poisson noise enabled the author to propose a method to isolate components from OSL decay curves with poor signal to noise ratios (SNR). To evaluate the efficacy of the approach this was applied to real geological situations. The samples from various situations ranging from Tsunami deposits, proximally transported sediments and the isolation of fast component of quartz from feldspar contaminated OSL decay were explored.

Contents

List of Figures	iv
List of Tables	vi
Chapter 1 Introduction	1
1.1 Motivation and background	1
1.2 Scope of the thesis	3
1.2.1 Retrieval of component from OSL with poor SNR	4
1.2.2 Study of partially bleached sediments	4
1.2.3 Isolation of quartz signal from feldspar contaminated sample	5
1.2.4 Components of quartz of different origin	5
1.3 Organization of thesis	6
References	7
Chapter 2 Luminescence Principle and Dosimetry	9
2.1 Introduction	9
2.2 Luminescence basics	9
2.3 Theoretical aspects of luminescence: Energy band model	10
2.4 TL phenomenon	14
2.5 OSL phenomenon	18
2.6 OSL models	19
2.7 OSL dosimetry	24
2.7.1 Natural OSL dosimeter: Quartz and feldspar	24
2.7.2 Stimulation and emission of quartz	27
2.7.3 Resetting of the OSL signal	29
2.7.4 Age determination	33
References	34
Chapter 3 Instrumentation and Experimental Protocols	38
3.1 Introduction	38
3.2 TL/OSL Measurement	38
3.2.1 Luminescence detection system	40
3.2.2 Stimulation sources	42
3.2.3 Irradiation source	43
3.3 Illumination and irradiation cross-talk	44
3.3.1 Irradiation cross talk	45
3.3.2 Illumination cross talk	46
3.4 Dose rate Measurement	49
3.4.1 Thick source α counting: U and Th concentration	49
3.4.2 Gamma spectrometry: K-40 concentration	50
3.4.3 Cosmic ray contribution	51
3.5 Evaluation of equivalent dose: D_e	51
3.5.1 Single Aliquot Regenerative method: SAR	52

3.5.2 Natural Correction Factor-SAR: (NCF-SAR)	53
3.5.3 Component Specific Dose -SAR: (CSD-SAR)	55
3.6 Sample preparation	55
3.7 Evaluation of errors in dose estimation	57
References	59
Chapter 4 Numerical Analysis of OSL	62
4.1 Introduction	62
4.2 Non-Linear fitting: Levenberg Marquardt method	63
4.3 Initial guess for Lev-Marq algorithm	65
4.4 Quality of fitting and validation of component	69
4.4.1 Sensitivity of model parameters: A comparative study	69
4.4.2 Analysis of residuals: Auto correlation	72
4.4.3 Chi-Square test	75
4.4.4 F-test	77
4.5 Error estimation of model parameters	77
4.6 Generation of growth curve for OSL component	80
4.7 Check list for isolation of OSL components	81
Reference	83
Chapter 5 Component Specific Study: Dating Perspective	84
5.1 Introduction	84
5.2 Review of earlier work	85
5.3 Relevance of OSL model parameters	86
5.4 Dependence of OSL parameters on dose and stimulation power	87
5.5 Numerical experiments on synthetic OSL profiles	88
5.5.1 Generation of synthetic OSL profile	88
5.5.2 Observations on synthetic OSL profiles	90
5.6 Observations on dose retrieved from different components	93
5.7 Quantifying interference of components	95
5.8 Case studies	102
5.8.1 Paleodose of partially bleached sediment: Tsunami sediment	102
5.8.2 Study of components of quartz from different sites	108
5.8.3 Component study of feldspar contaminated quartz	111
5.9 Conclusions	113
References	114
Chapter 6 Summary and future outlook	117
6.1 Summary	117
6.2 Future outlook	119
Appendix	122
Nonlinear least squares fit	122
Principle of maximum likelihood	122
Taylor method	124
Gradient method	127
References	129

List of Figures

- Figure 2.1 Schematic of quartz lattice with common defects (redrawn after Bøtter-Jensen et al. [5]) 12
- Figure 2.2 Energy band model of the luminescence phenomenon. a) Ground state with empty charge traps; b) ionizing radiation removes an electron from its parent atom and lifts it to the conduction band from where the electron is trapped; the remaining positive charge (electron-hole) is trapped at a hole trap; c) metastable state with occupied charge traps; d) the electron is liberated from its trap by thermal or optical stimulation and recombines with a hole center (luminescence center) under emission of luminescence (TL/OSL) (redrawn after Wagner [6]) 13
- Figure 2.3 TL glow curve on the basis of equation. It shows how term1 and term2 govern TL peak. 17
- Figure 2.4 A simplified electronic system depicting various transitions of charge within the system. Electrons and recombination centres are indicated by full circle and empty circle respectively. 20
- Figure 2.5 Plateau test to determine the stability of OSL signal from quartz. The region between 300-450 °C corresponds to stable signal as the ratio of TL intensities is constant (redrawn after Aitken [10]) 25
- Figure 2.6 Emission from quartz for various stimulation wavelengths (redrawn after Bøtter-Jensen et al. [34]) 27
- Figure 2.7 Emission spectra of several samples of sedimentary quartz from south-east South Australia aged from 0 to 800 ka, obtained for stimulation using the 647 nm line from a krypton laser (redrawn after Huntley et al. [37]) 29
- Figure 2.8 Various phenomena responsible for resetting of signal (redrawn after Wagner [6]) 30
- Figure 2.9 Bleaching of the 514.5 nm-stimulated luminescence by various wavebands of near infra-red and visible light. The bleaching curves are plotted against energy deposited in that waveband. The transects allow determination of the total energies required for 5%, 50% and 95% reduction of the OSL for any given waveband (redrawn after Spooner [35]) 31
- Figure 2.10 Spectrum of sunlight: outside the atmosphere and at sea-level with the sun 60° below zenith. The vertical scale gives the energy per

unit wavelength interval received per unit time by unit area of a horizontal surface facing upwards (redrawn after Aitken [10])	32
Figure 3.1 (a) Basic components of OSL detection. (b) Schematic of TL/OSL reader and its main components (redrawn after Bøtter-Jensen et al. [1])	39
Figure 3.2 PMT response curve. Maximum quantum efficiency occurs at 300-400 nm (redrawn after Bøtter-Jensen et al. [1]).	40
Figure 3.3 (a) Stimulation spectra of Blue-LED and the filter combinations used to detect the luminescence in UV region. (b) Stimulation spectra of IR-LED and the filter combinations used to detect the luminescence in blue region (redrawn after Bøtter-Jensen et al. [1]).	41
Figure 3.4 Schematic diagram illustrating illumination and irradiation cross talk	44
Figure 3.5 Illumination cross-talk increases with increasing illumination time. Result from Riso1 (TL-DA 12).	48
Figure 3.6 Protocol followed to measure irradiation and illumination cross talk.	48
Figure 3.7 (a) and (b) illustrate the estimation of dose by interpolation. Experimental protocols for SAR and NCF-SAR have been briefly summarized.	54
Figure 3.8 Flow chart illustrating various steps involved in sample preparation. After every chemical treatment the sample is washed with distilled water.	56
Figure 4.1 Peeling technique to get initial guess for Lev-Marq algorithm.	67
Figure 4.2 OSL decay modeled by sum of three exponentials.	68
Figure 4.3 Autocorrelation test to monitor the randomness of residuals (a) two components fitted to data (b) three components fitted to data (c) four components fitted to data and (d) five components fitted to data.	75
Figure 5.1 Invariance of decay rates of different component of OSL with respect to dose	87
Figure 5.2 (a) Synthetic OSL profile with three exponentials (b) Synthetic OSL profile with Poisson noise.	89
Figure 5.3 Spread in amplitudes and decay rates retrieved using Lev-Marq algorithm from synthetic OSL profile with known parameters $I(t) = 0.7e^{-2.2t} + 0.2e^{-0.5t} + 0.1e^{-0.02t}$. The colorbar indicates the value of	

χ^2 . Retrieved parameters show large scatter for intensity of 500 units and χ^2 is poor (panel a and b). As intensity increases retrieved parameters cluster about the known values (panel c and d). 91

Figure 5.4 Comparison in spread of amplitudes of fast component retrieved by Lev-Marq algorithm (4a and 4c) and by proposed algorithm (4b and 4d). Upper two figure 4a and 4b shows comparison for low intensities while lower two figure 4c and 4d for high intensities. 93

Figure 5.5 The growth curve for different components and SAR for seven disks where 75 Gy dose was given to sample 94

Figure 5.6 The events undergone by sediments prior to its deposition. The figure illustrate the development of signal at various stage 96

Figure 5.7 Protocol to study the bleachability characteristic of components. 101

Figure 5.8 Coastal area and the sampling localities (1-9). Horizontal lines indicate the run-up elevation. Dotted line indicates the 100 m depth contour. 103

Figure 5.9 Distribution of paleodoses measured using the SAR protocol. (b) Paleodose distribution using fast component of the OSL decay. 105

Figure 5.10 (a) Approximate bathymetry of the region. (b) Approximate bathymetry of the coast near Nagapattinam. The zone of most bleached sediments comprises sediments up to a depth of 10 m and in the intertidal zone. 106

Figure 5.11 (a) Transmission of light in coastal water with high turbidity. Notice that the transmission spans eight orders of magnitude. (b) Bleaching time required for a 50% reduction of OSL signal at various depths based on data provided by Aitken and Jerlove [26, 27]. 107

Figure 5.12 The histograms of decay rates from pure quartz, pure feldspar and quartz contaminated by 30% feldspar by weight. 112

List of Tables

Table 2-1	Some reported values of trap parameters E (trap depth) and s (frequency factor), and calculated lifetimes at 20°C for quartz using various methods	26
Table 3-1	Commonly used filter combinations to detect the luminescence emission from quartz and feldspar. ND filters are used to reduce the intensity when light output is high.	42
Table 3-2	Values of cross-talk reported by various workers	45
Table 3-3	Irradiation cross talk in percentage for 400 Gy. Here set denotes the result of an experiment carried out on 5 disks.	46
Table 3-4	Illumination cross talk in percentage for 1000 s. *No measurable cross talk found in Riso2 (TL-DA 15) even at nearest adjacent disk.	47
Table 4-1	Parameters isolated using Lev-Marq method along with peeling technique. The OSL considered here corresponds to a pond sample (PARB TL1) and initial intensity was around 10000 units.	68
Table 4-2	Different set of parameters giving same numerical value of model function	70
Table 4-3	Sensitivity of various parameters of multiexponential model used for isolation of OSL components. The parameters used were obtained after isolating a typical OSL curve. $I(t) = 81e^{-2.184t} + 12e^{-0.444t} + 7e^{-0.004t}$. Here sampling interval was 0.16 s and total time was 40 s.	71
Table 4-4	This table shows the value of χ^2 , Q and F for different number of component in OSL. The value of χ^2 does not change after 3 components and Q values deviate from 0.5.	76
Table 4-5	Value of inverse of Hessian matrix are presented. The diagonal elements of inverse of matrix are variance of parameters of isolated OSL components and off diagonal elements are covariance of parameters.	80
Table 5-1	Decay parameters of OSL components for different stimulation power error in data is standard deviation of 5 different disk	88
Table 5-2	Comparison of amplitudes retrieved from synthetic OSL by proposed approach	92

Table 5-3 Comparison of doses estimated for different illumination time by different components and SAR. Here error is standard deviation of 5 disks.	95
Table 5-4 Deviation in doses estimated by SAR and fast component for bleaching of 5s which equivalent to 10 mean life of fast component. Here the decay parameters of fast, medium and slow were 2.2, 0.44 and 0.04 respectively. The contribution of medium component was varied from 5 to 85%	99
Table 5-5 Effect of Geological dose in overestimation of dose as calculated by SAR and Fast component for various bleaching time. The geological dose is considered to be 100 units and burial dose is varied from 10 to 90.	99
Table 5-6 Dose estimated using fast component and SAR for various bleaching times. The relative difference considered here is with respect to the true dose of 50 Gy, that was given after bleaching 1000 Gy for different time duration.	101
Table 5-7 Paleodoses estimated using SAR and Fast component of OSL	104
Table 5-8 Values of model parameters of different OSL components of various sample from three different sites.	109
Table 5-9 Decay parameters of OSL components of quartz from eight different sites	110
Table 5-10 Details of sites from where sample was collected	110
Table 5-11 Effect of repeated cycle of sun bleaching and 1000 Gy irradiation on decay rates of OSL components.	111

Chapter 1

Introduction

1.1 Motivation and background

A study of recent Earth history requires a quantitative understanding of the timing, duration and the rates of processes leading to sediment erosion, transport, accretion and preservation. Such studies inform about the processes (climate and tectonics) that sculpt the surface of the Earth. A knowledge of time when a particular sedimentation/erosion event occurred in the past enables deduction of the time scales and recurrence intervals of basic geomorphic processes. Such reconstruction of the time series helps in determining the periodicities of the causative processes and thereby are likely to aid prediction of future climatic and tectonic events. Such an extrapolation relies heavily on the degree to which the past processes are resolved and hence, an accurate knowledge of time becomes an indispensable aspect of any such study. An ideal dating method would be the one that directly dates the material of interest i.e. that can be applied to the ubiquitous naturally occurring minerals viz. quartz and feldspars, covers a large time range, and provides calendar ages without a need for external calibration. Luminescence dating comes closest to satisfying these conditions [1, 2].

The potential application of Luminescence in radiation dosimetry was first suggested by Daniels et al [3]. By the early 1970's, thermoluminescence (TL) was an established method to determine the age of ancient ceramics [4, 5]. Huntley et al. [6] demonstrated another luminescence dating approach using Optically stimulated luminescence (OSL). This development revolutionized the studies on recent Earth history by its capabilities to provide ages of deposition of sediments using its constituent minerals [7, 8].

Minerals such as quartz or feldspar acquire a luminescence signal from the natural ionizing radiation namely α , β , or γ in a cumulative manner. The radiation dose and the induced luminescence are proportional. In nature, these ionizing radiations arise due to the decay of naturally occurring radionuclides viz., U, Th and K along with the cosmic rays. The major contribution comes from U, Th, and K while cosmic rays provide a minor, but finite contribution. The life time of these radionuclides is ~ billion years which ensures that the irradiation flux (dose rate) remains constant over million year time scales. This constancy implies that absorbed dose (also termed paleodose) is proportional to the exposure time of irradiation. The absorbed radiation dose is estimated by measuring the luminescence from the mineral and by converting it to radiation dose units by measuring the luminescence signal produced by known laboratory doses. The environmental dose rate is estimated by measuring the concentration of radionuclides, U, Th and K in the sediment and then using standard prescriptions [7, 9]. The ratio of paleodose and environmental dose rate provides the time elapsed (age) since the last zeroing of luminescence signal, i.e.

$$Age = \frac{Paleodose(D_e)}{Dose\ rate(\dot{D})} \quad (1.1)$$

The correctness of an age relies on the accuracy and precision with which the paleodose and dose rate are measured. Determination of true paleodose becomes critical when this technique is applied to the sediments. One of the key issues in luminescence dating is to ascertain that the luminescence was zero or near zero at

the time of deposition. For sediments, this occurs via photobleaching by natural daylight during the transport of minerals constituting the sediment. Exposure of minerals to the daylight results in a rapid photobleaching of luminescence signal. Complete erasure of geological luminescence requires typically a few minutes of clear daylight. Resetting of the signal depends on factors such as spectrum and flux of daylight, which is available to minerals during the transport. Barring resonance transitions, the bleaching efficiency depends on the energy (wavelength) and the flux [10, 11]. In natural geological settings, these factors vary considerably with depositional environment. In general, with a few exceptions, mineral grains in a sediment matrix are partially and heterogeneously bleached. Consequently there is a dose distribution in the sample at the time of deposition (residual dose). If this residual dose is not determined properly, overestimation of paleodose occurs and hence sediment age will be erroneous. So far this is handled by a variety of ways that include, simulation of bleaching conditions and using these to deduce the net residual, measuring luminescence from single grains and constructing a dose histogram to extract the signal of the most bleached grains using proper statistical formulations etc.

The present thesis aimed a slightly different approach of finding ways to mathematically isolate the most easy to bleach signal from a composite OSL, such that even in the most adverse depositional environments this signal can be assumed to have been bleached. A computational procedure to extract the most easy to bleach component was developed. Further, it was demonstrated that a robust age estimation can then be made in situation with residual doses and/or the presence of contaminated signals.

1.2 Scope of the thesis

This thesis explores the finer features of optically stimulated luminescence (OSL) decay and explores various components of this decay. This is based on the premise that each component arises from traps of different photoionization cross sections and follows an exponential decay [12]. A Matlab based program to isolate these exponentials from OSL decay curve comprising sum of exponentials,

was developed and rigorously tested. It was then demonstrated that component specific analysis of samples for OSL dating provides better results than conventional approaches. This thesis also explored other innovative applications involving the use of component analysis. A successful application of component specific study relies on correctness of the isolated components. Isolation of OSL components and their validation thus, formed a major part of this thesis. Besides this, the findings of numerical experiments on computer generated synthetic OSL profiles enabled us to propose a method to isolate the components from OSL with poor signal to noise ratio (SNR). This method was successfully tested in retrieving the low doses administered to the sample. A brief overview of the problems addressed using component specific analysis of OSL is presented in following section.

1.2.1 Retrieval of component from OSL with poor SNR

The present thesis examined the prospects of achieving component specific paleodose (CSD) estimation, particularly for the samples with poor signal to noise ratio. Noise here includes Poisson noise associated with photon counting statistics and the instrumental background. Typically instrumental background ranges from 50-100 count/sec. With these considerations, the maximum value of noise is typically 300 counts/sec. Levenberg-Marquardt algorithm [13, 14] was used to isolate the component of OSL and the resulting components were validated by various statistical tests viz. autocorrelation analysis of residuals, Chi-square test and F-test [15, 16]. The efficacy of Levenberg-Marquardt algorithm in retrieving the component was examined on numerically generated synthetic OSL profiles. These synthetic OSL profiles included Poisson noise. Detailed study on synthetic OSL profile enabled a suggestion for a possible solution for retrieval of the components from OSL with poor SNR.

1.2.2 Study of partially bleached sediments

A simulation experiment was performed to study the applicability of component specific studies in context of partially bleached samples. Study of the ratio of the

paleodose estimated by fast and medium component provides a means to identify partial bleaching in a sample. In a validation study, the laboratory prepared samples were dosed and the effect on paleodoses of fast and medium component was examined.

The component specific approach was then applied to Tsunami sample. The sediments transported by the 2004 tsunami, provided a maiden opportunity to verify the basic premises of the zeroing of the luminescence at the time of deposition. The comparative study of conventional single aliquot regeneration (SAR) method and component specific SAR (CS-SAR) suggested that (CS-SAR) provided more reliable estimates as compared to SAR, in such samples [17]. Further the CS-SAR consistently provided evidence that a fraction of sample was well bleached at the time of their deposition after transport with the tsunami wave.

1.2.3 Isolation of quartz signal from feldspar contaminated sample

In general, contamination of quartz OSL by the feldspar OSL can lead to erroneous estimation of dose. This is due to sensitivity changes suffered by feldspar during repeated cycles of heating and bleaching during measurements [18, 19] and anomalous fading [20-22]. Jain and Singhvi [23] tried to resolve this problem by pre IR cleaning. The possibility of estimating the dose acquired by such contaminated sample using component specific analysis was examined. Analysis of the components of quartz and feldspar OSL decay indicated that their fast components have distinctly different decay parameter. Studies in the present thesis suggested that the fast component of quartz can be isolated from OSL of a sample with contamination by feldspar. It is thus possible to avoid undesirable effect of feldspar OSL using mathematical isolation of the fast component of quartz.

1.2.4 Components of quartz of different origin

In this study, the behavior of different components was considered to examine the possibility of identifying any correlation between decay parameters of OSL component and the provenance of quartz. Analysis of various samples indicated

consistent presence of three components viz. fast, medium and slow with negligible variation in decay parameters for a given sample. This suggests a possible use of decay parameters of OSL for provenance studies.

1.3 Organization of thesis

This thesis is organized into six chapters as summarized below.

Chapter 2 presents basic concepts involved in luminescence dating. It includes a discussion on the theoretical aspects of luminescence phenomenon and the rationale of using a multiexponential model to describe OSL decay curve.

Chapter 3 discusses the instrumentations involved in OSL dating and summarizes protocols employed to estimate the dose. A detailed study on the illumination and irradiation cross talk in three Risoe TL-OSL readers is presented.

Chapter 4 deals with characterization and isolation of the component of OSL decay. The algorithm used to isolate the OSL components is described. Besides, various statistical tests to validate the components constituting OSL are discussed.

Chapter 5 provides a comprehensive assessment of OSL components. A strategy for separating components from OSL with poor SNR will be discussed. This approach is applied to partially bleached sediments, Tsunami sediment and sample contaminated by feldspar. Besides this, components of a large variety of quartz have been examined.

Chapter 6 presents a summary of the work in the thesis and outlines areas for future research.

References

1. Singhvi A. K., Wagner G. A., and Korisettar R., "Techniques in the chronometry of the Paleolithic (invited Review)", in *Early Human Behaviour In the Old World*, Petraglia M. and Korisettar R., Editors. 1998, Routledge Press, U.K. pp. 23-83.
2. Wagner G. A. (1998). "Age determination of young rocks and artifacts: Physical and chemical clocks in quaternary geology and archaeology" 1st ed. Springer Verlag: Berlin, pp 484.
3. Daniels F., Boyd C. A., and Saunders D. F. (1953). "Thermoluminescence as a research tool". *Science* **117**: pp 343-349.
4. Aitken M. J., Tite M. S., and Reid J. (1964). "Thermoluminescent dating of ancient ceramics". *Nature* **202**: pp 1032-1033.
5. Aitken M. J., Zimmerman D. W., and Fleming S. (1968). "Thermoluminescent dating of ancient pottery". *Nature* **219**: pp 442-444.
6. Huntley D. J., Godfrey-Smith D. I., and Thewalt M. L. W. (1985). "Optical dating of sediments." *Nature* **313**(5998): pp 105-107.
7. Aitken M. J. (1985). "Thermoluminescence Dating" ed. Academic Press: London, pp 359.
8. Aitken M. J. (1998). "An introduction to Optical dating" 1st ed. Oxford University press, USA: New York, pp 280.
9. Adamiec G. and Aitken M. (1998). "Dose Rate Conversion factors: Update". *Ancient TL* **16**(2): pp 37-49.
10. Berger G. W. (1990). "Effectiveness of natural zeroing of the thermoluminescence in sediments". *Journal of Geophysical Research* **95**(B8): pp 12375-12397.
11. Spooner N. A. and Questiaux D. G. (2000). "Kinetics of red, blue and UV thermoluminescence and optically-stimulated luminescence from quartz". *Radiation Measurements* **32**(5-6): pp 659-666.
12. Bailey R. M., Smith B. W., and Rhodes E. J. (1997). "Partial bleaching and the decay form characteristics of quartz OSL". *Radiation Measurements* **27**(2): pp 123-136.
13. Marquardt D. W. (1963). "An Algorithm for Least-Squares Estimation of Nonlinear Parameters". *SIAM Journal on Applied Mathematics* **11**(2): pp 431-441.

14. Venkatraman P. (2001). "*Applied Optimization with matlab programming*" ed. Wiley-interscience: New-york, pp
15. Grinvald A. and Steinberg I. Z. (1974). "On the Analysis of fluorescence decay kinetics by the method of Least-Squares". *Analytical Biochemistry* **59**: pp 583-598.
16. Bevington P. R. and Robinson D. K. (2002). "*Data Reduction and Error Analysis for the Physical Sciences*" 3 ed. McGraw-Hill Education: pp 352.
17. Murari M. K. and Singhvi A. K. "Component Specific paleodose estimation in optically stimulated luminescence dating : Methodology, Applications and Implications". in *APLD*. 2006. Hongkong.
18. Wallinga J., Murray A. S., and Bøtter-Jensen L. (2002). "Measurement of the dose in quartz in the presence of feldspar contamination". *Radiation Protection Dosimetry* **101**(1-4): pp 367-370.
19. Blair M. W., Yukihara E. G., and McKeever S. W. S. (2005). "Experiences with single-aliquot OSL procedures using coarse-grain feldspars". *Radiation Measurements* **39**(4): pp 361-374.
20. Prescott J. R. and Robertson G. B. (1997). "Sediment dating by luminescence: a review". *Radiation Measurements* **27**(5-6): pp 893-922.
21. Auclair M., Lamothe M., and Huot S. (2003). "Measurement of anomalous fading for feldspar IRSL using SAR". *Radiation Measurements* **37**(4-5): pp 487-492.
22. Spooner N. A. (1992). "Optical dating: Preliminary results on the anomalous fading of luminescence from feldspars". *Quaternary Science Reviews* **11**(1-2): pp 139-145.
23. Jain M. and Singhvi A. K. (2001). "Limits to depletion of blue-green light stimulated luminescence in feldspars: implications for quartz dating". *Radiation Measurements* **33**(6): pp 883-892.

Chapter 2

Luminescence Principle and Dosimetry

2.1 Introduction

This chapter presents basic concepts involved in luminescence dosimetry. It starts with a brief introduction to luminescence which includes a description of various type of luminescence and an overview of the underlying physical principles. Then a discussion on the models proposed to explain the luminescence emission from materials is presented. Optically Stimulated Luminescence (OSL) and Thermally Stimulated Luminescence (TSL)/Thermoluminescence(TL) phenomena are then explained along with a discussion on the use of multiexponential model to describe the nature of OSL decay. Finally, a discussion on the basic principle of OSL dosimetry/dating is presented. This section also includes a discussion natural radiation dosimetry.

2.2 Luminescence basics

Luminescence is the emission of light on external stimulation. It is exhibited by a many materials ranging from inorganic to organic and from solids to liquids. The physical origin of luminescence in each of these materials is different but a

common feature is the emission of electromagnetic radiation resulting from a transition of an ion, molecule, or a crystal from an excited electronic/molecular state to a ground state [1, 2]. A transition can occur in two possible ways. One involving, deactivation of excited electronic state. This type of transitions is radiative and leads to emission of light in visible to UV region. The other possible channel of deactivation is via interaction with the lattice or transfer of energy to other ions. Such transitions do not produce light and are called radiationless transitions [1, 3]. The intensity and duration of luminescence are the aspects that distinguish it from other type of stimulated radiations. In other words the luminescence radiation is in excess as compared to that of thermal radiation of heated bodies.

In general, luminescence emission involves an excitation of the ground state electrons of solids to an excited state and eventual emission either spontaneous or delayed. Depending upon the delay between excitation and emission of light, luminescence is broadly classified into fluorescence and phosphorescence. In case of fluorescence, the time delay between the absorption of energy and emission of light is less than 10^{-8} s, whereas time delay for phosphorescence is greater than 10^{-8} s, In other words fluorescence emission takes place nearly simultaneously with absorption of radiation and stops immediately once the radiation ceases [1]. Photoluminescence, cathodoluminescence, bioluminescence, chemiluminescence and triboluminescence etc. are the examples of fluorescence, while thermoluminescence and optically stimulated luminescence fall under the category of phosphorescence.

2.3 Theoretical aspects of luminescence: Energy band model

The energy band model was suggested for the materials which involves movement of charge carrier thorough the crystal lattice prior to recombination [4, 5]. These charge carriers are produced when crystals are exposed to ionizing radiation like α , β and γ radiation whereby the energy is transferred to the atoms of the solids. Main processes involved include ionization, Compton scattering, photoelectric

and pair production. These interactions finally results in producing free electrons and heating of solids.

Kronig-Penny model forms the basis for band theory of solids. In this model electron is subjected to a periodic array of potential wells as in case of solids where lattice atoms lie in close proximity. This model predicts that the allowed energies of electrons lie only in allowed zones and the allowed energy values are separated by band gaps. In other words, the energy spectrum of electron in a crystal comprises allowed energy bands. The highest energy band filled with electrons is termed as valence band and the subsequent higher energy band is called conduction band. The occupancy of each band is described by the density of states function.

$$N(E) = Z(E)f(E)$$

$$f(E) = \frac{1}{e^{\frac{E-E_f}{kT}} + 1} \quad (2.1)$$

Where $N(E)$ is the density of occupied energy levels, $Z(E)$ is the density of the available energy states, $f(E)$ is the Fermi Dirac distribution function and E_f is the Fermi level. It is clear from equations (2.1) at absolute zero temperature the energy levels below E_f are filled while those above E_f are empty. In case of insulator and semiconductors E_f lies above the topmost valence energy level. Hence at absolute zero temperature the valence band is entirely full while conduction band is empty. Depending on the position of fermi level (E_f) in band gap, the crystal can be categorized into insulator, semiconductor and metal. For ideal insulators, the density of available energy states $Z(E)$ is zero between conduction and valence band. However, the presence of defect or impurities within the lattice causes breakdown in periodicity of the crystalline structure and new localized energy states are created in the forbidden gap [2]. These intermediate energy states in forbidden gap are called traps. Common defects and imperfections that occur in crystal are illustrated in Figure 2.1.

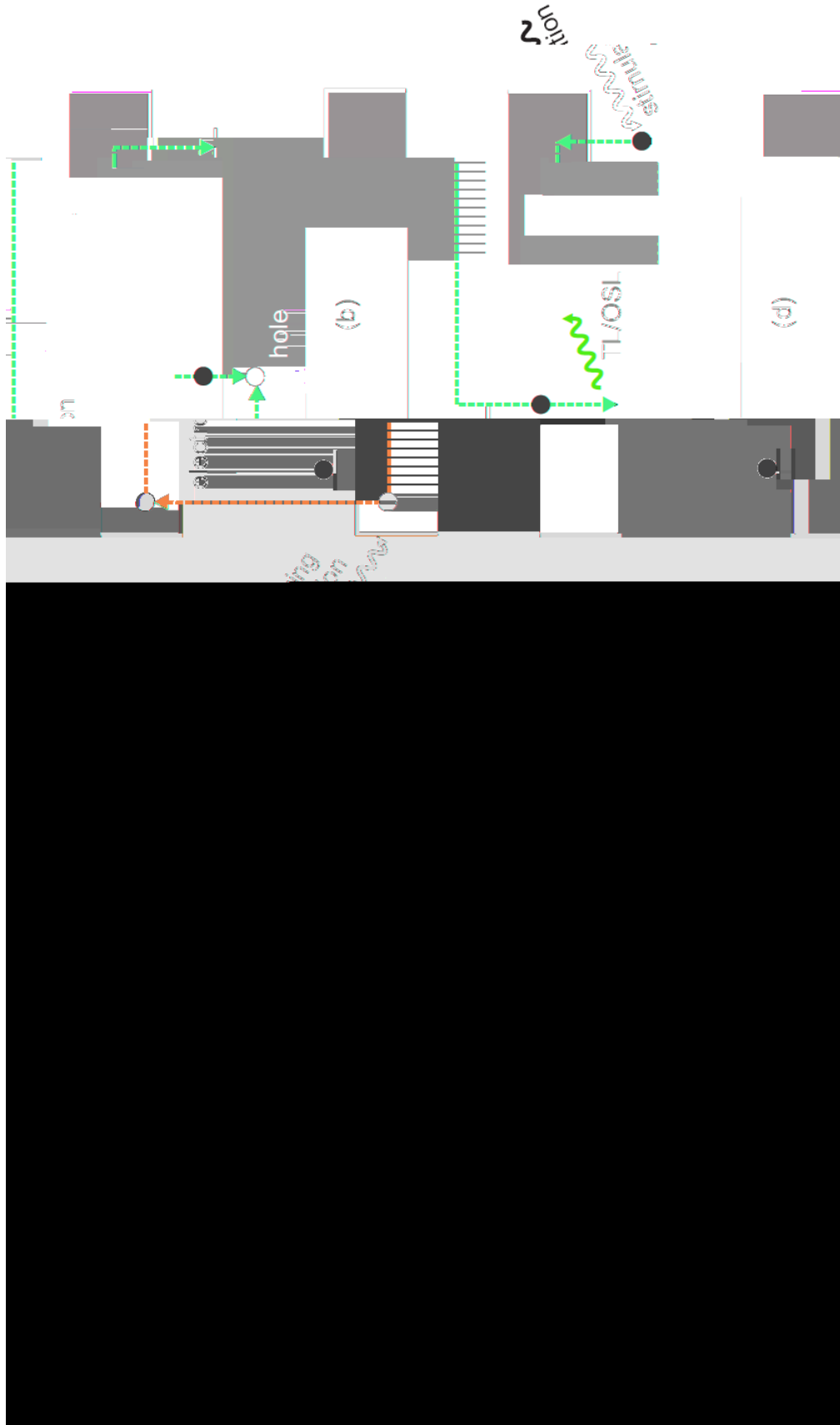


Figure 2.2 Energy band model of the luminescence phenomenon. a) Ground state with empty charge traps; b) ionizing radiation removes an electron from its parent atom and lifts it to the conduction band where the electron is trapped; the remaining positive charge (electron-hole) is trapped at a hole trap; c) metastable state with occupied charge traps; d) the electron is liberated from its trap by thermal or optical stimulation and recombines with a hole center (luminescence center) under emission of luminescence (TL/OSL) (redrawn after Wagner [6])

Charge traps in the crystal play a prominent role in luminescence processes. When ionizing radiation interacts with crystal, electrons and holes are generated. A fraction of these charges gets trapped at various lattice defects [7]. The life time of these trapped charges is decided by the charge environment at its trapping site i.e. binding energy of trapped charge. An appropriate stimulation can however cause instantaneous detrapping of these charges. Some of these charges radiatively recombine at an appropriate trap centres (recombination centres) causing luminescence. Figure 2.2 elucidates various stages of luminescence emission process.

Various kind of luminescence exists depending upon the source of excitation and stimulation. However, the major part of present work deals with OSL and TL of natural quartz and feldspar. Physical principles involved in TL and OSL phenomena are briefly discussed next.

2.4 TL phenomenon

The single trap model introduced by Randall and Wilkins [8], offers a simplified explanation for TL phenomenon. This model explains the relation between the shape of the TL curve and the various physical parameters involved in the Luminescent crystal. the model considers a single type of electron trap center with activation energy E , concentration N and a single radiative recombination center.

The model is based on the following assumptions.

1. The crystal has a single trap level within the forbidden gap between valance and conduction band.
2. The thermally stimulated electrons from the trap have negligible chance of being retrapped.

At a given instance the charge carrier population in a crystal is governed by Boltzmann statistics [4]. At temperature T , the fraction of trapped electrons making a transit to conduction band is $n e^{-E/kT}$ and hence the detrapping rate of electrons can be expressed as

$$-\frac{dn}{dt} \propto ne^{-\frac{E}{kT}} \Rightarrow -\frac{dn}{dt} = sne^{-\frac{E}{kT}} \quad (2.2)$$

$$\tau = s^{-1} e^{\frac{E}{kT}} \quad (2.3)$$

Where k is Boltzmann constant, T is ambient temperature, n is concentration of electrons in traps, τ is the life time, s is frequency factor and E is the energy depth of the trap relative to the conduction band.

Equation (2.3) suggest that the time spent by electron in a trap is governed by ambient temperature T , trap depth E and the frequency factor s . If $E \gg kT$ then the residence time of electron in trap becomes extremely long. For example, if $E = 1.5\text{eV}$, $s = 10^{12}$ per sec and $T = 27^\circ\text{C}$ the residence time of electron will be 7.3×10^5 years [2]. From dosimetry/dating perspective, a trap must have an adequate depth to ensure the stability of charges over long storage time. The effect of lattice vibrations can be expressed in terms of frequency factor. From quantum mechanical considerations, the frequency factor (s) is given by

$$s = \nu \kappa e^{\frac{\Delta S_{entropy}}{k}} \quad (2.4)$$

Here ν is collision frequency of an electron with the lattice, κ is transition probability of trapped charges and $\Delta S_{entropy}$ is change in entropy associated with the transition of charges from the trap to the conduction band. Typically s has values comparable to lattice vibration frequencies $\sim 10^{12}$ - 10^{14} s⁻¹ [4].

In practice thermoluminescence is a measurement of emitted photon flux as a function of temperature and the resulting plot is termed as glow curve. In order to have an estimate of the shape of glow curve, equation (2.3) is written in terms of temperature. Assuming linear heating rate, time t and temperature T are related as follows

$$\begin{aligned}\frac{dT}{dt} &= q = \text{constant} \\ \Rightarrow T &= qt + c_0\end{aligned}\tag{2.5}$$

Where c_0 is constant of integration and q is the heating rate. The glow curve intensity (I) that results when charges, released from trap by heating, recombine with hole in the recombination centres, is given by the following relation

$$I = -c \frac{dn}{dt}\tag{2.6}$$

Where c is constant. Now equations (2.3), (2.5) and (2.6) together yield

$$I(T) = cn_0 s e^{-\frac{E}{kT}} e^{-\int_{T_0}^T \frac{s}{q} e^{-E/kT'} dT'}\tag{2.7}$$

The above expression comprises two exponential terms. The first exponential term governs the rising part of glow curve while the second exponential term governs the falling of glow curve. For low temperatures the second term approaches unity and hence the initial rise is essentially decided by first term. At high temperatures the second term becomes prominent causing the decay of intensity. The interplay of these terms gives a bell shape structure (Figure 2.3).

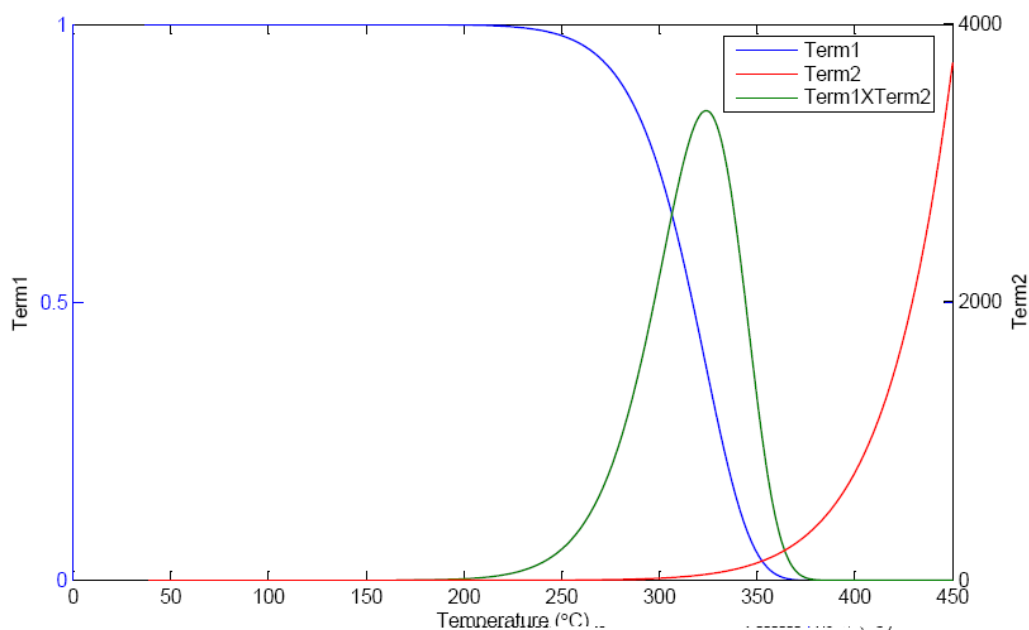


Figure 2.3 TL glow curve on the basis of equation. It shows how term1 and term2 govern TL peak.

In the present formulation the probability of stimulated electron to recombine at luminescent centre is considered at 1 and no retrapping is assumed. This is first order kinetics. Cases involving retrapping are described by second order or mixed order (general order) kinetics. A general expression for TL intensity involving general order kinetics [2] is given by

$$I(T) = cs' n_0 e^{-(E/kT)} \left[1 + \frac{s'(\alpha-1)}{q} \int_{T_i}^T e^{-(E/kT')} dT' \right] \quad (2.8)$$

Where α is order of kinetics and s' is modified frequency factor. The value of α determines the kinetics of stimulated electron. $\alpha = 1$ is first order kinetics where the released carrier does not return to trap and $\alpha = 2$ describes a case where the stimulated electron has an equal probability of retrapping and recombining.

Equations for TL intensity suggest an intimate relation between a trap depth and the occurrence of intensity maximum. Generally, a phosphor contains a number of traps at various trap depths. Thus a glow curve consists of a number of glow peaks, each corresponding to different trapping levels. In general, the life time of

for dating/dosimetry purpose [9, 10]. Every phosphor has specific TL glow peaks

Some of the common glow peaks in quartz occur at 110

electron in deeper traps is longer as compared to that of electrons in shallower traps. The glow peaks occurring at temperature less than 200°C are generally considered unstable at environmental temperature and therefore are not suitable

°C, 220°C, 325°C and luminescence intensity
375°C. Similarly for feldspar the peaks occur at 110°C, 280°C, 320°C and 350°C. In case of quartz and feldspar 325°C and 285°C glow-peaks have the requisite stability for dating/dosimetry applications.

2.5 OSL phenomenon of OSL the charges are optically evicted from their

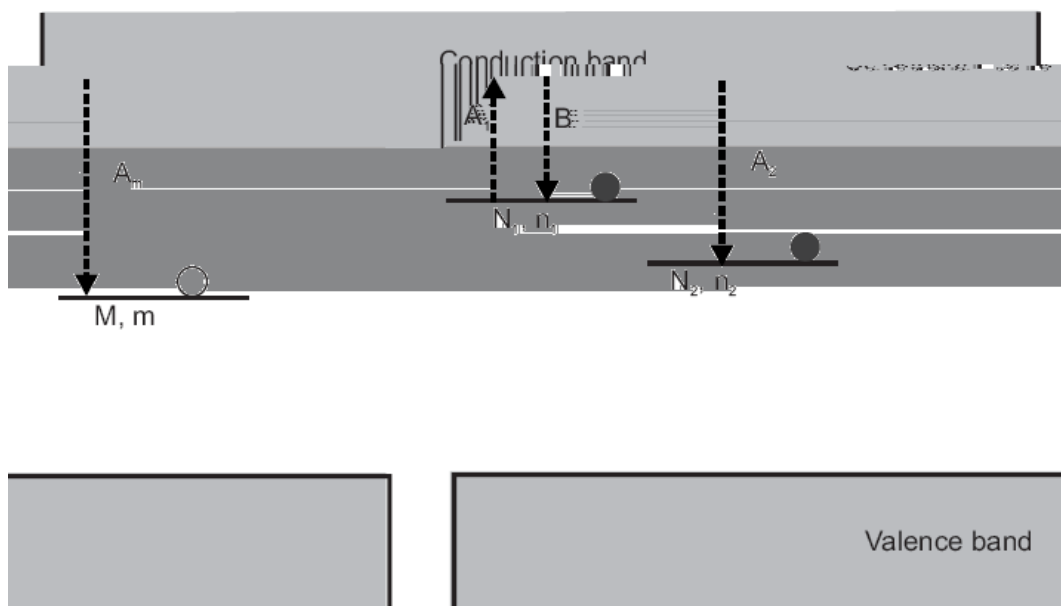
The physical principal of OSL and TL are similar with the exception that in case

In view of above, OSL has been a preferred method for the dating of sediments and in the radiation dosimetric application [6]. OSL has several variants and

exponential decay either due to re-trapping of charges or due to the presence of the multiple optically active traps or both.

Bailey et al [12], suggested that the contribution of re-trapping to the multi-exponential nature of OSL is significant only when any of the traps or recombination centre approaches saturation. Even if re-trapping is allowed the OSL decay becomes slower but remains exponential. However, it is reported that when traps are far from saturation level, the resulting OSL exhibits non-exponential nature thereby suggesting the existence of multiple traps leading to non exponential nature of OSL.

To explain the shape of OSL decay, a simplified model consisting of two types of trap and single recombination centre is considered. Energy band diagram of this model is presented in below Figure 2.4



recombination centre. Further, to emulate the possible kinematics of electrons in crystal 1) two types of trap were considered one of which was optically active (N_1) while other was optically inactive (N_2) 2) retrapping of electrons is allowed for both types of traps.

Detrapping rate of electrons from N_1 type of traps due to optical excitation is taken as B . The released electron is excited to conduction band and can be captured at each of the possible site denoted by N_1 , N_2 and M . The probabilities of electron capture at each of these sites are A_1 , A_2 and A_m respectively. If n_c is free electron concentration in conduction band, the traffic of electrons in the crystal is governed by the following rate equations.

$$\frac{dn_1}{dt} = -Bn_1 + n_c(N_1 - n_1)A_1 \quad (2.9)$$

$$\frac{dn_2}{dt} = n_c(N_2 - n_2)A_2 \quad (2.10)$$

$$\frac{dn_c}{dt} = Bn_1 - n_c(N_1 - n_1)A_1 - n_c(N_2 - n_2)A_2 - n_cmA_m \quad (2.11)$$

$$\frac{dm}{dt} = -n_cmA_m \quad (2.12)$$

To simplify the above rate equations following assumption are made

1. N_1 & n_1 and N_2 & n_2 . This means that available concentration of traps is much higher than the trapped electron concentration i.e. traps are not saturated by electrons.

2. Hole concentration m is assumed to be a large number so that every detrapped electron has large recombination probability.

3.

Quasi-equilibrium condition assumed, i.e. there is no charge accumulation

in conduction band $\frac{dn_c}{dt} \approx \frac{dn_1}{dt}, \frac{dn_2}{dt}, \frac{dm}{dt}$ i.e. $\left| \frac{dn_c}{dt} \right| \approx 0$

Assumptions 1 and 2 reduces the rate equation to the below form

$$\frac{dn}{dt} = -Bn + n_c A_{n_1} \tag{2.13}$$

$$\frac{dn}{dt} = -n A_{n_2} \tag{2.14}$$

$$\frac{dn_c}{dt} = B - n_c A_{n_1} - n_c A_{n_2} - n_c A_{m_1} \tag{2.15}$$

$$\frac{dm}{dt} = -n_c A_{m_1} \tag{2.16}$$

Where $A_{n_1} = (N_1 - n_1)A_1$, $A_{n_2} = (N_2 - n_2)A_2$ and $A_{m_1} = m.A_m$

Applying 3rd and 4th assumption to equation (2.12), (2.14) and (2.16)

$$\frac{dn_1}{dt} = -Bn \left[1 - \frac{A_{n_1}}{A_n + A_{n_1} + A_{m_2}} \right] \tag{2.17}$$

Charge neutrality condition is satisfied i.e. $n + n^+ = m$.

4.

$$\frac{dm}{n_1} = \frac{B n_1 A_{m_1}}{n_2 m_1}$$

2.7 OSL dosimetry

The simple dependence of OSL intensity on dose has found application in diverse fields like personal radiation dosimetry, accident dosimetry geological and archeological dating, in radiation diagnostic imaging etc. The present work mainly deals with dosimetry of natural radiation environment and its use in determining the timing of past geological events. This geochronological method for dating is unique due to its ability to date geological formation using mineral grains (quartz, feldspar) that constitutes the sediment. This fact eliminates many sources of errors of interpretation of ages, seen in most other methods.

2.7.1 Natural OSL dosimeter: Quartz and feldspar

A dosimeter is a device that measures or evaluates the energy deposited by ionizing radiation to the medium. A dosimeter can be a direct or indirect dosimeter depending on the principle involved in measurement of radiation dose. For a device to qualify as a dosimeter it must possess some physical property that depend on radiation and is reproducible. Major requirement of environmental dosimeters are, high sensitivity, stability with respect to time at ambient temperature, accuracy and precision, linear response within dynamic range of dosimeter and high reproducibility. In case of geochronology quartz and feldspar are the indirect dosimeters. Here, the luminescence emitted by these minerals provides a measure of the dose of radiation absorbed by the mineral. By calibrating of the luminescence signals against known doses of radiation, the luminescence yield is converted to absorbed dose.

Feldspars and quartz are the most widely occurring minerals in earth crust and both of these are sensitive OSL dosimeters. Thus they are widely accepted natural OSL dosimeter for dating of geological sediment. The choice of the mineral that is being used usually depend on the availability within a sample, and the age of the sediments. Quartz saturates at lower doses than feldspars, and so the use of feldspar might prove to be advantageous for dating older deposits. In context of OSL dosimetry stability of signal refers to the capability of traps to retain the signal without any degeneration over time. The major degenerative mechanisms are

separate stable and unstable luminescence. To avoid interference of unstable luminescence in OSL, the unstable traps before the TL plateau region are emptied by pre-heating the sample prior to OSL measurement. Table 2-1 presents the trap depth and lifetime of associated electrons for quartz as reported by various workers by different methods.

Signal	Trap depth (E)	Freq. factor (s)	Life time ()	Reference
OSL	1.84 eV	$2.0 \times 10^{15} \text{ s}^{-1}$	$6.0 \times 10^8 \text{ a}$	Smith et al. [15]
OSL	1.65 eV	$2.7 \times 10^{13} \text{ s}^{-1}$	$2.8 \times 10^7 \text{ a}$	Huntley et al. [16]
OSL	1.59 eV	$2.8 \times 10^{12} \text{ s}^{-1}$	$2.1 \times 10^7 \text{ a}$	Spooner and Questiaux [17]
OSL	1.66 eV	$1.0 \times 10^{13} \text{ s}^{-1}$	$1.1 \times 10^8 \text{ a}$	Murray and Wintle [18]
TL (325 C)	1.69 eV	$1.0 \times 10^{14} \text{ s}^{-1}$	$3.0 \times 10^7 \text{ a}$	Wintle [19]
TL (325 C)	1.60 eV	$5.7 \times 10^{12} \text{ s}^{-1}$	$1.7 \times 10^7 \text{ a}$	Spooner and Questiaux [17]

Table 2-1 Some reported values of trap parameters E (trap depth) and s (frequency factor), and calculated lifetimes at 20°C for quartz using various methods

Studies by Smith et. al. [15], suggest that the 325 °C TL peak and the OSL peak are correlated. This suggest implicitly that the mean life of the signal is $\sim 10^7$ a. Thus, OSL signal from quartz is sufficiently stable to permit dating over the entire time range of the quaternary. Thus the upper limit of the dating is now determined by signal saturation, rather than thermal fading.

2.7.1.2 Athermal fading: Anomalous fading

The usage of feldspar is limited owing to the anomalous fading [20-24] and long term fading. Feldspar also changes its sensitivity during multiple OSL readout [25]. In general for deep traps, the lifetime of electrons should be large and hence thermal decay is insignificant. However, in case of feldspar, it has been observed that there is a leakage of luminescence signal from the deeper traps even at room temperature. This decay of luminescence signal was initially termed as ‘anomalous’ fading and later explained being due to quantum tunneling of charges to nearby recombination centers [26-30]. Anomalous fading causes serious underestimation of age. Typically, the signal loss follows a logarithmic decay over the laboratory time scale e.g., more than 1 year in Lamothe and Auclair [31] and this restricts the usage of feldspar to younger samples. For

quartz, Wintle [20] did not observe any loss in TL during storage for 2 years. Similar observations were made on OSL of quartz by Roberts et al. [32] and no loss in OSL was detected even after 70 days of storage at room temperature. The general inter-comparisons suggest that quartz does not exhibit anomalous fading.

Optimization of the Luminescence measurement necessitates the study of stimulation and emission spectrum of the mineral of dosimetric interest. Such studies of the stimulation spectrum not only allow the selection of a specific mineral, but also provide an optimized stimulation wavelength to maximize luminescence efficiency. An extensive study in this area [33, 34] has shown that the OSL intensity (I) increases with decreasing stimulation wavelength (increasing energy), as is shown in Figure 2.6.

As seen in figure there is a change in slope in the wavelength region 500-520 nm. The appearance of this knee is still poorly understood and it is recommended to avoid this wavelength region for stimulation. Further studies on quartz have shown that the stimulation by wavelength exceeding 690 nm is inefficient in producing luminescence [35] while shorter wavelength ($< 450\text{nm}$) is avoided because in this wavelength range there is interference between emission (360-440nm) and stimulation wavelength of quartz. Widely used stimulation

wavelengths for quartz are green and blue (514nm and 470nm) [36]. In case of feldspar infrared stimulation was found to be most efficient.

Spectral characteristics of luminescence emitted from quartz helps select the most appropriate detection window for dosimetry. The fact that different emissions might have different characteristics (stability, bleachability or dose-response) makes it all the more important to pursue such studies. Luminescence emissions of quartz with 647 nm stimulation suggest the presence of single emission band centred at 365 nm (Figure 2.7).

Similar emission band was observed with green light (514 nm) stimulation. Extensive work on TL emission spectra has shown three main quartz TL emission bands at 360- 420 nm (near UV-violet), at 420-490 nm (violet-blue) and at 600-650 nm (orange-red). The probable luminescence centre giving rise to the OSL emission has been identified by [38, 39] as the $[\text{H}_3\text{O}_4]^\circ$ centre. Using Electron Spin Resonance (ESR) and TL, they were able to show that two point defects namely $[\text{AlO}_4]^\circ$ and $[\text{H}_3\text{O}_4]^\circ$ are responsible for the TL signal at $\sim 100^\circ\text{C}$.,. However, only the $[\text{H}_3\text{O}_4]^\circ$ recombination centre yields emission at 380 nm, comparable to the OSL emission.

hence overestimation of age. The Figure 2.10 schematically illustrates the various possible ways of resetting the signal of sediment.

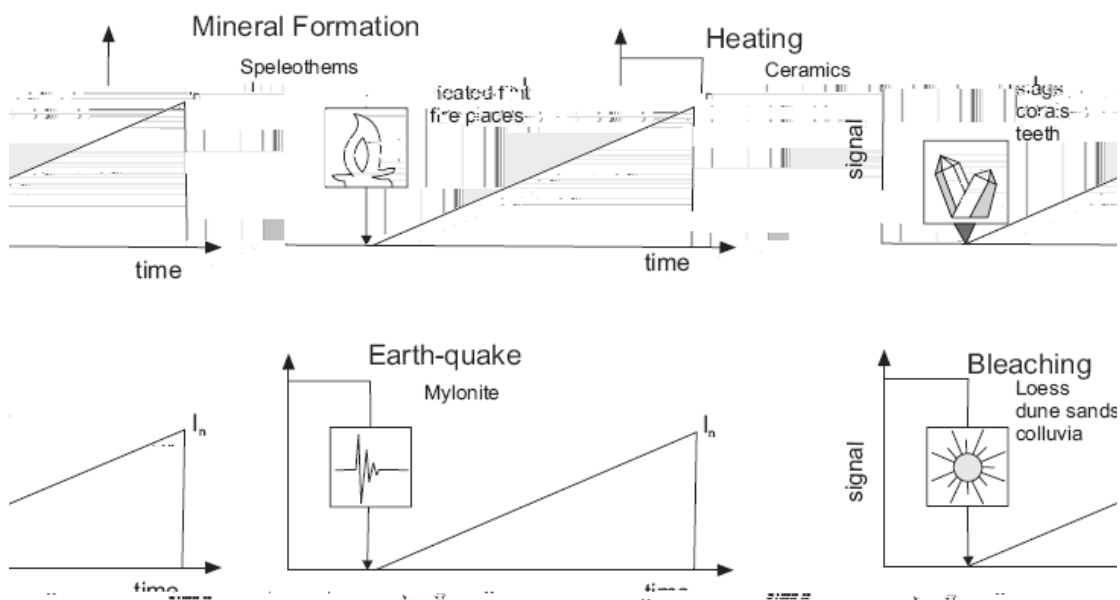
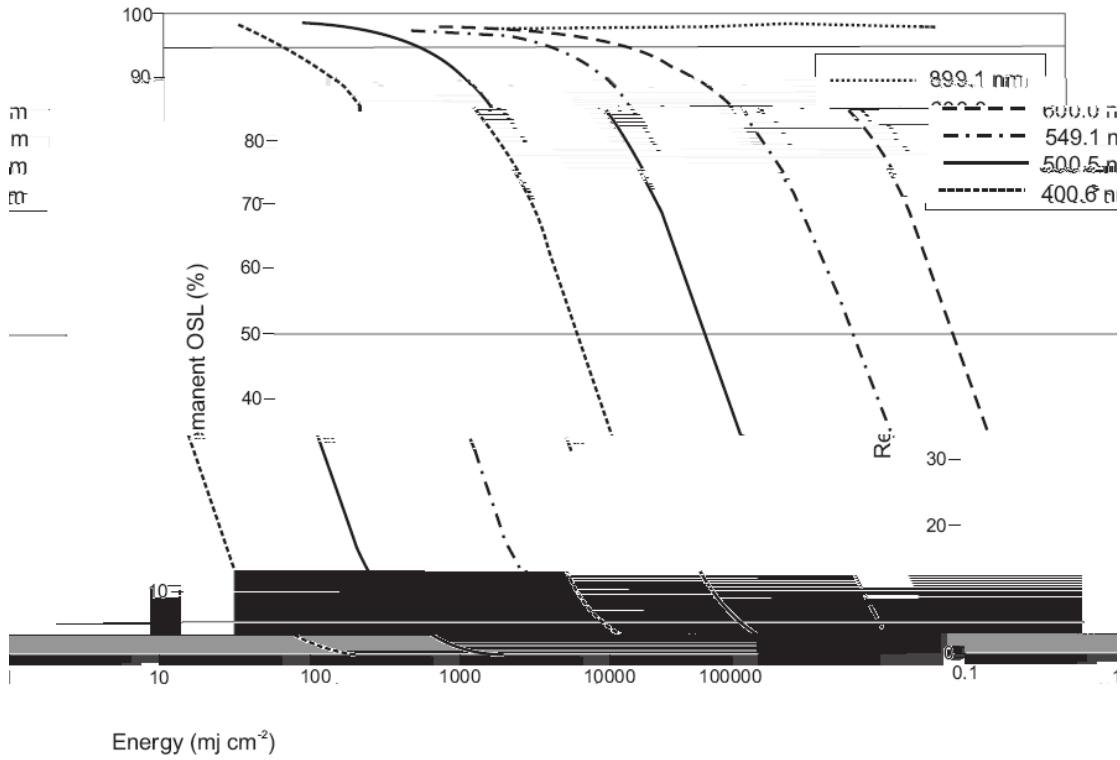


Figure 2.8 Various phenomena responsible for resetting of signal (redrawn after Wagner [6])

As seen in figure, apart from mineral formation where the signal is abinitio zero, the resetting of signal can take place by heating, exposure to light and by pressure. The figure also shows the corresponding geological events that can be dated. Resetting of signal by heating is relevant in archaeological events while optical bleaching occurs in transportation of sediment by wind or water. The heat generated during tectonic events may lead to resetting of signal of sediment. Thus OSL dating can also be used for tectonic faults. The temperature involved in heating-events, archeological and tectonic faults are sufficiently high enough to cause near complete thermal zeroing of the signal.

However, in case of sediments where resetting is due to exposure to sunlight, the zeroing of signal depends on the factors like light intensity, the spectrum and duration of the exposure. A number of authors have obtained evidence for satisfactory resetting of wind transport sediments (that see full daylight during transport) [40-43]. Evidences for poor bleaching have also been found in several studies [14, 44-48]. Studies by Spooner [35] have shown a strong dependence of

bleaching on the stimulation wavelength. Figure 2.9 shows the bleaching efficiency of various wavelengths.



Figure

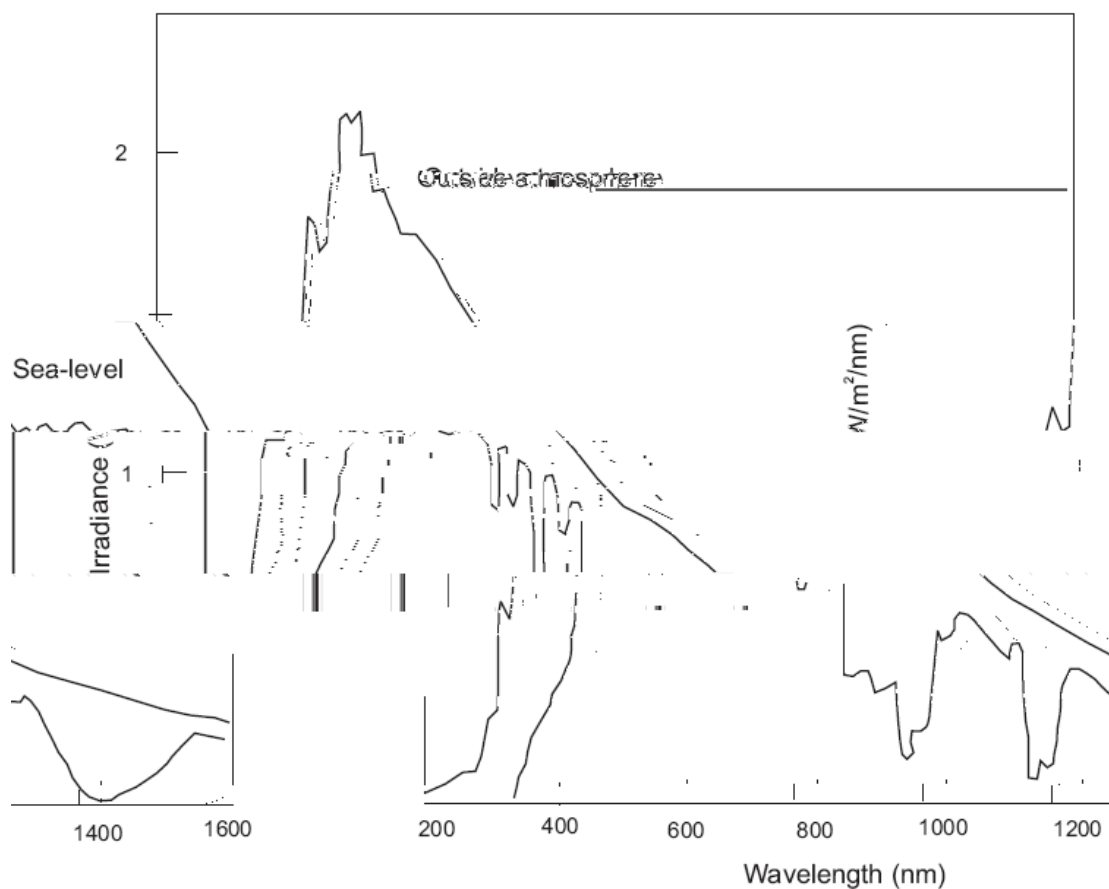


Figure 2.10 Spectrum of sunlight: outside the atmosphere and at sea-level with the sun 60° below zenith. The vertical scale gives the energy per unit wavelength interval received per unit time by unit area of a horizontal surface facing upwards (redrawn after Aitken [10])

However, complete resetting of the signal from sediment is not always possible. For depositional environments that have short transport durations (e.g. colluvial), and/or where there is considerable attenuation and filtering of the solar spectrum, the assumption of complete resetting becomes increasingly difficult to achieve. For example, in fluvial environments the higher photon energy part of the spectrum is strongly attenuated through water [44]. In context of determining true burial dose, the significance of partial resetting signal from the perspective of OSL component has been explored in greater detail in Chapter 4 and Chapter 5 of this thesis.

2.7.4 Age determination

Measurement of the naturally accumulated OSL and calibration of this signal using the OSL signal following known laboratory radiation doses allows an estimate of the paleodose (D

e). Paleodose is the laboratory dose required to produce the luminescence in resetting at the burial time. The OSL signal is directly related to the burial period. In principle, once the environmental dose rate is calculated, the age (burial period) of

$$\frac{\text{Lum Acquired (L)}}{(\quad)} = \frac{\text{Equivalent dose (D}_e\text{)me}}{(\quad)}$$

14. Bailey R. M. and Arnold L. J. (2006). "Statistical modelling of single grain quartz De distributions and an assessment of procedures for estimating burial dose". *Quaternary Science Reviews* **25**(19-20): pp 2475-2502.
15. Smith B. W., Rhodes E. J., Stokes S., and Spooner N. A. (1990). "The Optical Dating of Sediments Using Quartz". *Radiat Prot Dosimetry* **34**(1-4): pp 75-78.
16. Huntley D. J., Short M. A., and Dunphy K. (1996). "Deep traps in quartz and their use for optical dating". *Canadian Journal of Physics* **74**(3-4): pp 81-91.
17. Spooner N. A. and Questiaux D. G. (2000). "Kinetics of red, blue and UV thermoluminescence and optically-stimulated luminescence from quartz". *Radiation Measurements* **32**(5-6): pp 659-666.
18. Murray A. S. and Wintle A. G. (1999). "Sensitisation and stability of quartz OSL: Implications for interpretation of dose-response curves". *Radiation Protection Dosimetry* **84**(1-4): pp 427-432.
19. Wintle A. G. (1975). "*Journal International* 4
20. Wintle A. G. (1973). "

40. Huntley D. J., "odfrey-Smith D. I., and Thewalt M. L. W. (1985). "Optical dating of sediments." *Nature* **313**(5998): pp 105-107.
41. Stokes S. (1992). "Optical dating of young (modern) sediments using quartz: Results from a selection of depositional environments". *Quaternary Science Reviews* **11**(1-2): pp 153-159.
42. Berger G. W., "Progress in luminescence methods for quaternary sediments", in *Dating methods for quaternary deposits*, Rutter N. W. and Catto N. R., Editors. 1995, Geological Association of Canada, GEOText **2**. pp. 81-104.
43. Duller G. A. T. and Bøtter-Jensen L. (1996). "Comparison of optically stimulated luminescence signals from quartz using different stimulation wavelengths". *Radiation Measurements* **26**(4): pp 603-609.
44. Berger G. W. (1990). "Effectiveness of natural zeroing of the thermoluminescence in sediments". *Journal of Geophysical Research* **95**(B8): pp 12375-12397.
45. Rhodes E. J. and Pownall L. (1994). "Zeroing of the OSL signal in quartz from young glaciofluvial sediments". *Radiation Measurements* **23**(2-3): pp 581-585.
46. Olley J., Caitcheon G., and Murray A. S. (1998). "The distribution of dose as determined by optically stimulated luminescence in small aliquots of Fluvial quartz: Implications for dating young sediments". *Quaternary Geochronology* **17**: pp 1033-1040.
47. Arnold L. J., Bailey R. M., and Tucker G. E. (2007). "Statistical treatment of fluvial dose distributions from southern Colorado arroyo deposits". *Quaternary Geochronology* **2**(1-4): pp 162-167.
48. Thomsen K. J., Murray A. S., Bøtter-Jensen L., and Kinahan J. (2007). "Determination of burial dose in incompletely bleached fluvial samples using single grains of quartz". *Radiation Measurements* **42**(3): pp 370-379.

Chapter 3

Instrumentation and Experimental Protocols

3.1 Introduction

This chapter details instrumentation and protocols used in luminescence studies presented in the thesis. Section 3.2 de

3.2.1 Luminescence detection system

A Photomultiplier tube along with suitable detection filter coupled to a photon counting system constitute the detection system. Detection filters shield PMT from scattered stimulation light and help to select a desired spectral window. The light sensitive component in the PMT is the cathode which is coated with a photo-emissive material like CsSb or other bialkali material. The PMT used in the TL/OSL luminescence reader was a bialkali EMI 9235QA PMT. It has maximum detection efficiency at approximately 400 nm, making it suitable for detection of luminescence from both quartz and feldspar. Figure 3.2 gives the quantum efficiency as a function of incident photon wavelength for this PMT. The PMT is operated in photon counting mode. To optimize the light detection, the distance between the PMT and the sample is kept small. As the stimulation sources are placed between the sample and the PMT, the sample-to-PMT cathode distance in the Riso TL/OSL luminescence reader is 55 mm, giving a detection solid angle of approximately 0.4 steradians [1, 2].

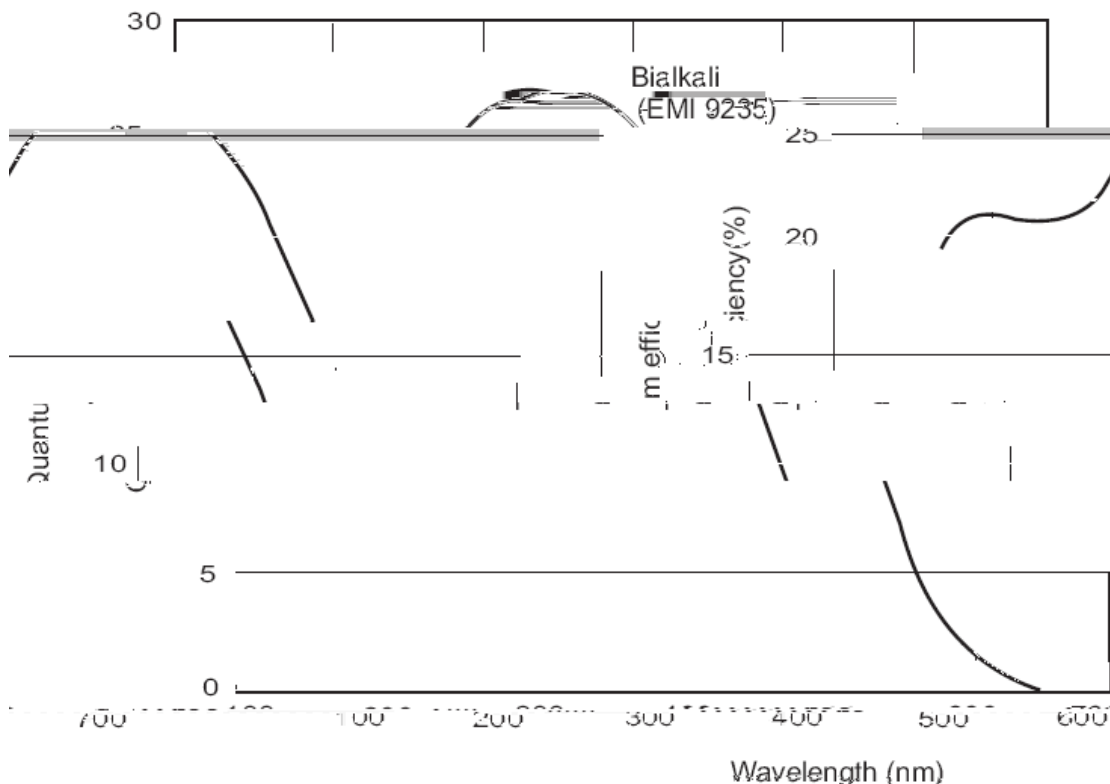


Figure 3.2 PMT response curve. Maximum quantum efficiency occurs at 300-400 nm (redrawn after Bitter-Jensen et al. [1]).

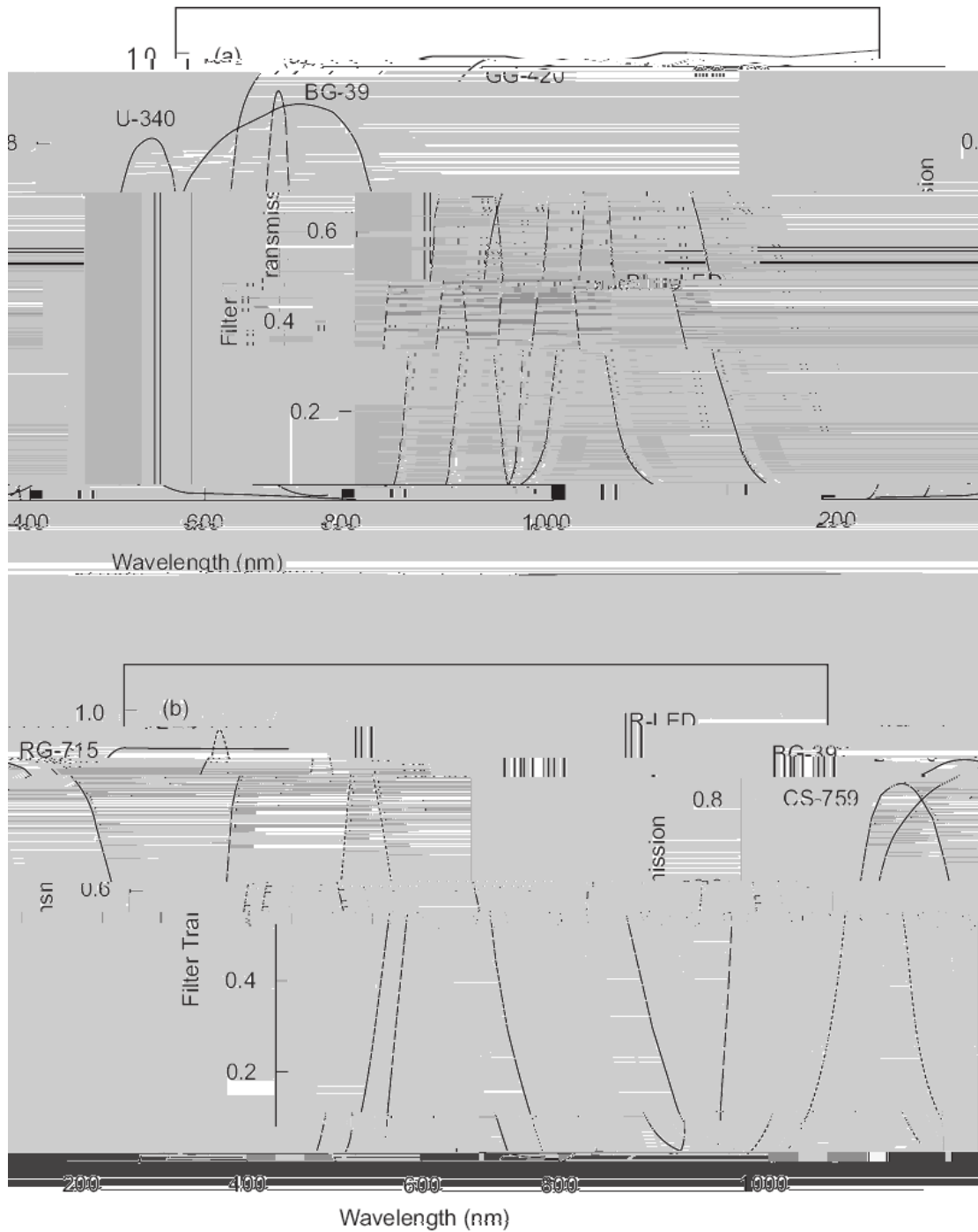


Figure 3.3 (a) Stimulation spectra of Blue-LED48 and the filter combinations used to detect the luminescence in UV region. (b) Stimulation spectra of IR-LED4 and the filter combinations used to detect the luminescence in blue region (redrawn after Böttger-Jensen et al. [1]).

The intensity of the stimulation light is several orders of magnitude larger than the emitted luminescence (typically stimulation light flux $\sim 10^{15}$ photon/cm²-sec) Thus, even minute fraction of scattered stimulation light entering can mask the pristine luminescence signal. Various color glass filters are used to prevent the interference of stimulation light. Quartz has a OSL emission centered on 365 nm and feldspars have a emission centered on 410 nm (violet) [3, 4]. Table 3-1 summarizes commonly used filters. Figure 3.2 and Figure 3.3 show the transmission curves of filter combinations and PMT quantum efficiency as function of wavelength.

Mineral	Wavelength (nm)		Filter Combination		
	Emission	Stimulation	Cut off Filters	Detection Filters	Neutral Density Filter
Quartz	~365, ~470	GLSL (430-520)	GG-495	Hoya U 340	ND
Quartz	~365	BLSL (470)	GG-420	Hoya U 340	ND
Feldspar	~410	IRSL (875)	Shott BG-39	Corning Cs 7-59/5-58	ND

Table 3-1 Commonly used filter combinations to detect

quartz at the sample position is ~ 0.1 Gy/s (Riso TL-DA 12), 0.066 Gy/s (Riso TL-DA 15). The source is mounted on a pneumatically controlled holder with a graded shielding of carbon, aluminum and lead. Source takes ~ 0.11 s to rotate from the closed position to the open position [8]. The distance between the source and the sample is 5 mm. A 0.125 mm beryllium window is placed between the irradiator and the measurement chamber. This window separates beta source from the measurement chamber.

3.3 Illumination and irradiation cross-talk

Cross talk is measure of illumination and irradiation received by the disk adjacent to the measurement disk. Cross-talk introduces systematic errors in paleodose leading to erroneous age estimation of the samples. The effect is particularly severe for young samples [9]. Cross irradiations delivers the dose to the neighboring discs and hence lead to overestimation of dose while cross illumination causes reduction of the signal in neighboring disks which leads to underestimation of dose. Schematic of the cross-talk sdows the positioning of the adjacent and measurement discs in Figure 3.4.

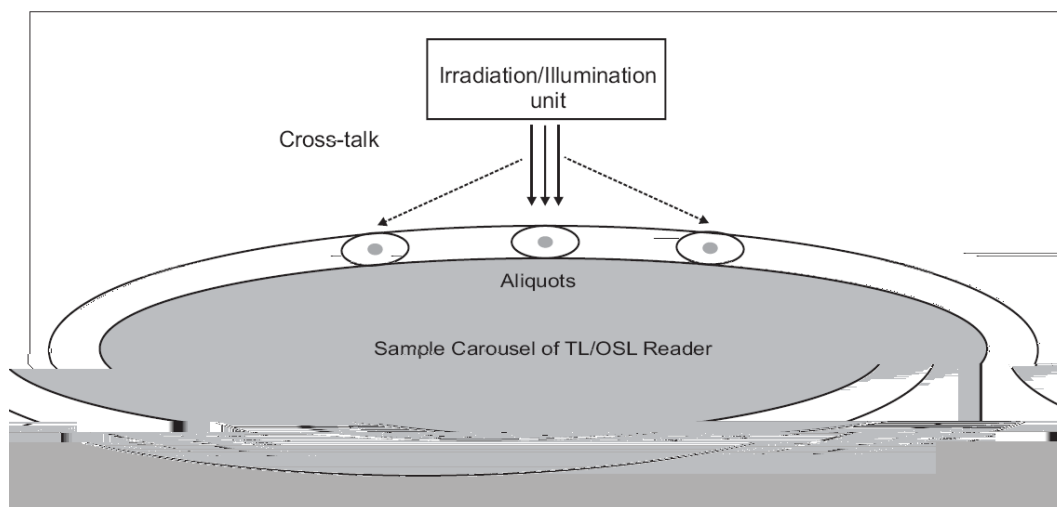


Figure 3.4 Schematic diagram illustrating illumination and irradiation cross talk

The Riso Automated TL/OSL reader is capable of a programmed readout cycle of up to 48 stations present on the carousel. The measurement protocol involves repeated irradiation and illumination of the individual aliquots. In the previous

work on cross-talk Markey et al [8] expressed illumination cross-talk as percentage of the equivalent stimulation time on the adjacent sample and irradiation cross-talk as percentage of dose received by an adjacent non-irradiated disk during the irradiation on measurement disk. Here loss of signal and dose received by adjacent disk were determined using the single aliquot regeneration (SAR) protocol. Bray et al [9] alternatively expressed illumination cross talk as percentage reduction in the signal of adjacent disk due to illumination on measurement disk. This cross-talk was also expressed in terms of equivalent stimulation time using short shine measurement.

In all of the work mentioned above the reported values of the crosstalk were very less as compared to the values obtained from an experiment conducted on the Riso TL/OSL reader Table 3-2. Besides this, the measurement protocols used by various workers [2, 8-10] to quantify the one of the above mentioned cross-talks did not take into account the interference due to another cross-talk (eg. one must consider the illumination cross talk during measurement of irradiation cross-talk). In view of this, the measurement protocols were modified to quantify the two cross-talks distinctly.

Carousal type	Illumination Cross talk		Irradiation cross talk		References
	Illumination time (s)	Cross- talk (%)	Dose (Gy)	Cross- talk (%)	
24	Not reported	Not reported	60 0042	Markey et al. [8]	
48	Not reported	Not reported	132	0060	Markey et al. [8]
24	Measured in terms of power	0.013	Not reported	0.04	Bøtter-Jensen [2]
48	Measured in terms of power	0.006	Not reported	0.17	Bøtter-Jensen [2]
48	4000	59.1	1000	0.0005	Bray et al. [9]

Table 3-2 Values of cross-talk reported by various workers

3.3.1 Irradiation cross talk

Five discs (n1, n2, M, n4 and n5) of 3 mm dia sample of high sensitivity Australian quartz were prepared and placed at different positions (1, 2, 3, 4 and 5). These disks were bleached by giving 100 sea blue light illumination at 200 °C. Following this, disc M placed at station 3 was irradiated using ⁹⁰Sr/⁹⁰Y beta for

400 Gy. The discs (n1, n2, n4 and n5) placed at stations (1, 2, 4 and 5) were moved to the stations (1, 5, 9 and 13) to

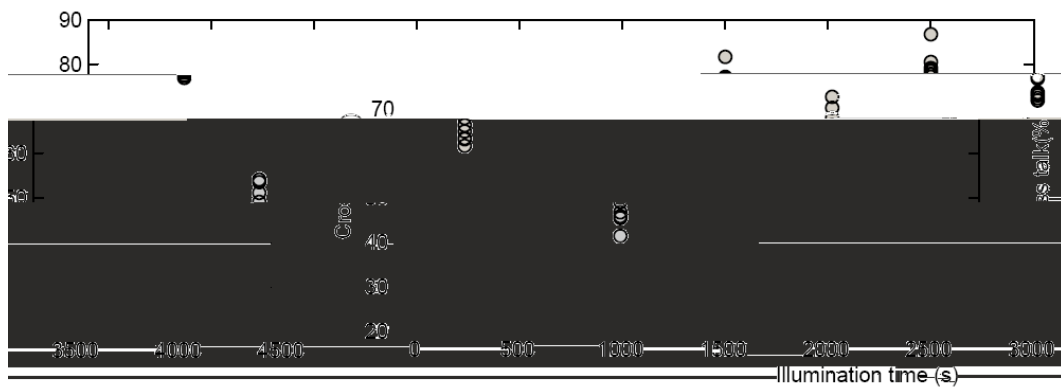


Figure 3.5 Illumination cross-talk increases with increasing illumination time. Result from Risol (TL-DA 12).

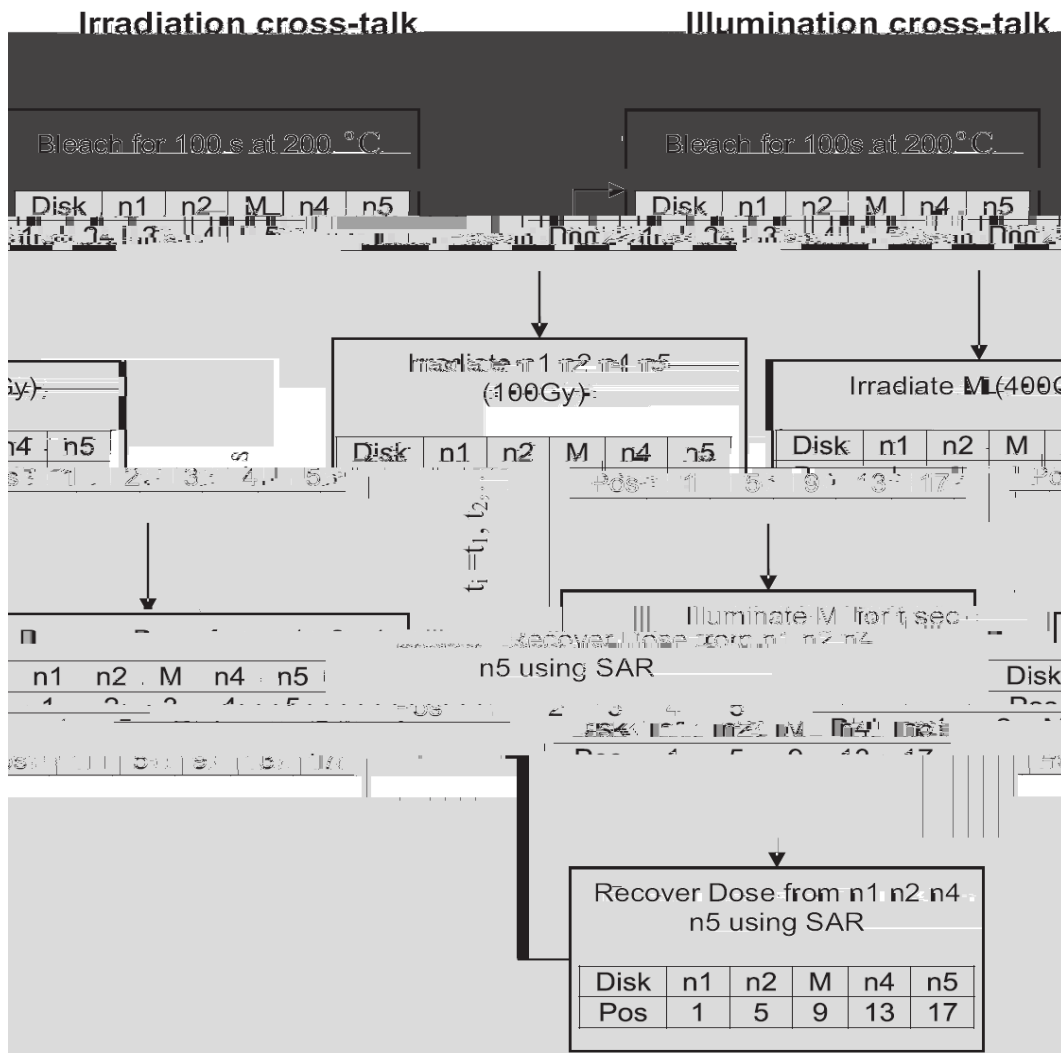


Figure 3.6 Protocol followed to measure irradiation and illumination cross talk.

Total number of alpha counts per ksec from 42 mm sample =

Total number of slow pair counts per ksec from 42 mm dia. sample =

Total number of alpha counts per ksec for Th and U can be estimated using the following relation from 42 dia sample

$$D_{Th} = 21 p \frac{0.38 D_s}{10^3} \quad (3.3)$$

$$D_U = D_{Th} D \quad (3.4)$$

Concentration of U and Th in ppm can be calculated using conversion factor suggested by [14].

$$U_c = \frac{D_U}{1.65} \text{ ppm} \quad (3.5)$$

$$Th_c = \frac{D_{Th}}{0.502} \text{ ppm}$$

In above calculations, the decay series of U and Th are considered in equilibrium ($N_1 = N_2 = \dots = N_i = N_j$). However, disequilibrium may take place mainly due to loss of Rn ($t_{1/2} = 3.83 \text{ d}$) from uranium 238 decay series. In such cases, hyper pure Germanium (HP Ge) Planar detector is used to detect any kind of disequilibrium by measuring γ activity from different members of the decay chain. This detector can detect even 300 keV energy gamma photons which enable to resolve the different gamma energy peaks of different isotopes. It is housed within a 10 cm thick lead shield of 0.025 cpsm for K.

3.4.2 Gamma spectrometry: K-40 concentration

In gamma spectrometry well type thallium (TI) activated sodium iodide crystal and lithium doped hyper pure germanium crystal were used to measure the K concentration in the sample. Thallium (TI) activated sodium

Iodide [NaI(Tl)] crystal is a scintillation detector which produces scintillation according to the energy of gamma photon. To measure K-40 concentration, the compton subtracted photo peak corresponding to 1.46 MeV gamma photon emissions were used. Approximately 10g of sample vials and Perspex spacers were used in the well to ensure identical counting geometry. The concentration of D-40 was estimated by comparing the photon counts with those from standard pure KCl. Typical photon counts along with background for KCl standard and samples are ~58 cpm and ~3 cpm respectively. The expression to calculate concentration of D-40 (%) is given below.

$$K_{sample} \% = \frac{(cnts / time / mass)_{sample} - BKG}{(cnts / time / mass)_{std} - BKG} \times K_{std} \% \quad (3.6)$$

Where cnts are the compton subtracted photopeak counts corresponding to 1.46 MeV γ -ray. K_{sample} and K_{std} are the potassium concentration of sample and standard respectively.

3.4.3 Cosmic ray contribution

Most of the cosmic ray absorbed by the earth's atmosphere however the secondary particles mainly muons contribute to the dose rate. These particles show a dependency on altitude and geographical latitude due to earth magnetic field. Therefore the cosmic dose rate was calculated as a function of altitude and latitude using equations given in [16].

3.5 Evaluation of equivalent dose: D_e

Equivalent dose measurement methods can be broadly classified into two categories, viz the additive and the regenerative dose method. Both these methods involve construction of luminescence signal vs radiation dose growth curve. In additive dose method radiation dose is added to the natural dose (sample as received) and natural dose is extrapolated to zero luminescence from the growth curve while in regenerative dose method the natural signal is compared with the

signal regenerated by laboratory irradiation and natural dose is estimated by interpolation. These methods are further classified into multiple aliquot additive/regenerative (MAAD/MAAR) and

3.5.2 Natural Correction Factor-SAR: (NCF-SAR)

In conventional SAR measurement protocol, sensitivity changes are corrected for every regeneration doses by normalizing them with subsequent test doses. But Singhvi et al [17] suggested that the change in sensitivity during the natural OSL measurement itself is not accounted by the SAR protocol [11]. For many samples a saturation was seen for laboratory doses whilst the natural signal was way beyond the saturation limit. This implies that there is change in sensitivity during the measurement of natural. To correct this sensitivity change a method to monitor 110°C TL peak by giving a small test dose to the sample before and after measurement of natural signal (figure 3.5b). If there is any change in sensitivity then the ratio of 110°C TL peaks (TL_1/TL_2) will show the deviation from unity. This ratio of TL peaks is used as correction factor for sensitivity changes.

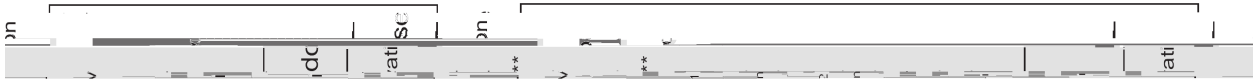


Figure 3.7 (a) and (b) illustrate the estimation of dose by interpolation. Experimental protocols for SAR and NCF-SAR have been briefly

3.5.3

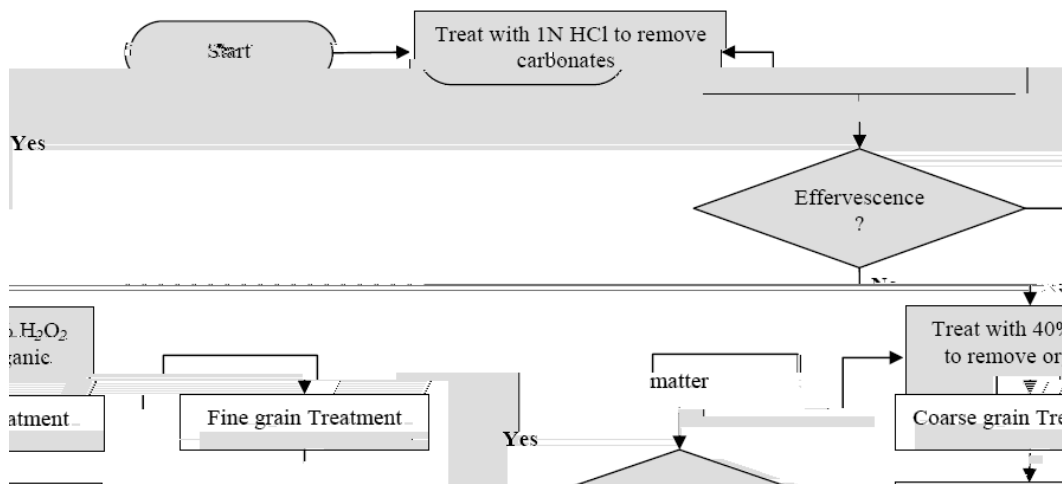


Figure 3.8 Flow chart illustrating various steps involved in sample preparation. After every chemical treatment the sample is washed with distilled water.

Generally, the coarse grain technique deals with pure quartz and feldspar minerals with grain size 90-125 μm or 150-200 μm while the fine grain technique deals with polymineralic assemblages, with grain size 4-11

the exception of H₂SiF₆) [22]. Since feldspar responds to IR stimulation, fine grain technique is often used in conjunction with IR stimulation to study the luminescence signal corresponding to feldspar alone. A flowchart depicting the procedure followed to separate the grains of interest from sediment samples is presented in Figure 3.8

3.7 Evaluation of errors in dose estimation

Usually dose acquired by sample is estimated using SAR protocol. Here growth curves (dose response curve) are constructed and the natural dose is estimated by interpolation. Background subtracted normalized intensities are used to construct growth curves and hence each point of the growth curve is given by

$$(X_i, Y_i) = f \left(\beta_i, \frac{L_i}{T_i} \right) \quad (3.7)$$

$$L_i = L_i^{sig} + L_i^{bg} \text{ and } T_i = T_i^{sig} + T_i^{bg}$$

Where β_i is the dose given to the sample, L_i^{sig}

$$\frac{L_i}{i} \sqrt{\frac{L_i^{sig} L_i^{bg}}{\left(\begin{matrix} sig \\ i \end{matrix} \begin{matrix} bg \\ i \end{matrix}\right)^2}}$$

References

1. Bøtter-Jensen L., McKeever S. W. S., and Wintle A. G. (2003). "Optically stimulated luminescence dosimetry" 1 ed. Elsevier Science: Amsterdam, Netherlands, pp 374.
2. Bøtter-Jensen L., *Development of optically stimulated luminescence techniques using natural materials and ceramics, and their application to retrospective dosimetry*. Science. 2000, University of Copenhagen: Copenhagen. pp. 186.
3. Huntley D. J., Godfrey-Smith D. I., and Haskell E. H. (1991). "Light-induced emission spectra from some quartz and feldspars". *Nuclear Tracks and Radiation Measurements* **18**(1-2): pp 127-131.
4. Krbetschek M. R., Gotze J., Dietrich A., Trautmann T., and Radiation Measurements Vol. N. p. (1997). "Spectral information from minerals relevant for luminescence dating". *Radiation Measurements* **27**(5/6): pp 612-619.
5. Bøtter-Jensen L. and Murray A. S. (1997). "Optically stimulated luminescence techniques for dating and retrospective dosimetry". *Radiation Measurements* **27**(5/6): pp 612-619.

25. Galbraith R. (1993). "Statistical models for mixed ages". *International Journal of Radiation Applications and Instrumentation. Part D. Nuclear Tracks and Radiation Measurements* **21**(4): pp 600-573.
26. Galbraith R. F. (1988). "Graphical display of estimates having different standard errors". *Technometrics* **30**: pp 271-281.
27. Galbraith R. F. (1990). "The radial plot: Graphical assessment of spread in ages". *International Journal of Radiation Applications and Instrumentation. Part D. Nuclear Tracks and Radiation Measurements* **17**(3): pp 207-214.
28. Galbraith R. F. and Green P. F. (1990). "Estimating the component ages in a finite mixture". *International Journal of Radiation Applications and Instrumentation. Part D. Nuclear Tracks and Radiation Measurements* **17**(3): pp 197-206.
29. Lepper K., Larsen N. A., and McKeever S. W. S. (2000). "Equivalent dose distribution analysis of Holocene eolian and fluvial quartz sands from Central Oklahoma". *Radiation Measurements* **32**(5-6): pp 603-608.
30. Lepper K. and McKeever W. S. (2002). "An objective methodology for dose distribution analysis". *Radiation Protection Dosimetry* **101**(1-4): pp 349-352.

Chapter 4

Numerical Analysis of OSL

4.1 Introduction

The CW-OSL from quartz and feldspar can be expressed as the sum of exponentials [1-3] and are termed as the components of OSL decay. The present chapter deals with characterization and isolation of these OSL components. There are many numerical methods such as the nonlinear least squares fit, graphical peeling or curve stripping method, the Prony method, the method of modulating functions, the method of moments, the Laplace-Pade approximation, the Tikhonov regularization method, the Gardner transformation, the method of maximum entropy and others [4] for exponential analysis. However, considering the fact that the nonlinear least squares method is simple, easy-to-implement, efficient and commonly used method for fitting nonlinear models to the experimental data, it was employed for the present studies. Further, various statistical tests were carried out to validate the isolation of OSL components.

4.2 Non-Linear fitting: Levenberg Marquardt method

In present thesis the Levenberg Marquardt (*Lev-Marq*) algorithm was used. This method for isolation of components is based on Gradient and Taylor methods. The present section discusses this algorithm and appendix provides more details on the Gradient and Taylor method. *Lev-Marq* algorithm combines good features of Gradient and Taylor methods. Here, initially the *Gradient* method is used and then the algorithm switches to the Taylor method when the minimum of χ^2 is approached [4-6]. The mathematical form of the multiexponential model to be fitted to the OSL data is

$$\hat{I}(t) = \sum_{i=1}^M a_i e^{-t/\tau_i} \quad (4.6)$$

$$(a_1, a_3, a_5, \dots)$$

(a_2, a_4, a_6, \dots) of components.

Taylor Method: This method minimizes χ^2 based on below expression

$$\sum_{j=1}^n H_{ij} \delta a_j = \frac{\partial \chi_0^2}{\partial a_i} \quad (4.4)$$

Here $\frac{\partial \chi_0^2}{\partial a_i}$ represents partial derivative of χ^2 evaluated at initial guess of model parameters (a_i^0). δa_j is the small increment in initial guess for model parameters and $H_{ij} \equiv \frac{\partial^2 \chi^2}{\partial a_i \partial a_j}$ are the elements of Hessian matrix H which shows the curvature of χ^2 surface.

Gradient Method: This method minimizes χ^2 using the expression

$$\begin{aligned} \delta a_i &= -\frac{1}{\beta H_{ii}} \frac{\partial \chi_0^2}{\partial a_i} \\ \Rightarrow \beta H_{ii} \delta a_i &= -\frac{\partial \chi_0^2}{\partial a_i} \\ \Rightarrow \beta \sum_{j=1}^m H_{ij} \delta a_j \delta_{ij} &= -\frac{\partial \chi_0^2}{\partial a_i} \end{aligned} \quad (4.5)$$

Where δ_{ij} is 1 if $i = j$ and 0 otherwise, δa_i is the small increment in model parameters.

a large value is assigned to β and this is subsequently reduced in each iteration expecting χ^2 to decrease. For sake of brevity the set of model parameters a_1, a_2, a_3, \dots is represented by a parameter vector \hat{a}^{χ_0} . *Lev-Marq* algorithm comprises following steps

1. Choose an appropriate initial guess \hat{a}^{χ_0} .
2. Compute χ^2 at initial guess \hat{a}^{χ_0}
3. Solve equation (4.6) with a large value of β to obtain the vector $\delta \hat{a} = (\hat{a}^{\chi_{new}} - \hat{a}^{\chi_0})$ and compute χ^2 at $\hat{a}^{\chi_{new}}$.
4. If $\chi^2(\hat{a}^{\chi_{new}}) \geq \chi^2(\hat{a}^{\chi_0})$ decrease β by 10 (or any other large number) and return to step 3.
5. Check convergence criterion. If $|\chi^2(\hat{a}^{\chi_{new}}) - \chi^2(\hat{a}^{\chi_0})| < 0.001$ then $\hat{a}^{\chi_{new}}$ is the optimized set of parameter and stop else increase β by factor of 10 and go to step 3.

4.3 Initial guess for Lev-Marq algorithm

$$I = I_3(t) = a_3 e^{-\lambda_3 t} \quad (4.8)$$

Taking log on both sides of equation (4.8)

$$\ln I_3(t) = \ln(a_3) - \lambda_3 t \quad (4.9)$$

Thus a straight line fit to experimental data for large t provides a reasonable estimate of λ_3 and a_3 . Subsequently the exponential with next higher λ can then be isolated by subtracting the appropriate computed data corresponding to λ_3 . Repeating this procedure an approximate estimate of the parameter of all the exponentials involved in the experimental data is achieved. Figure 4.1 provides a typical result.

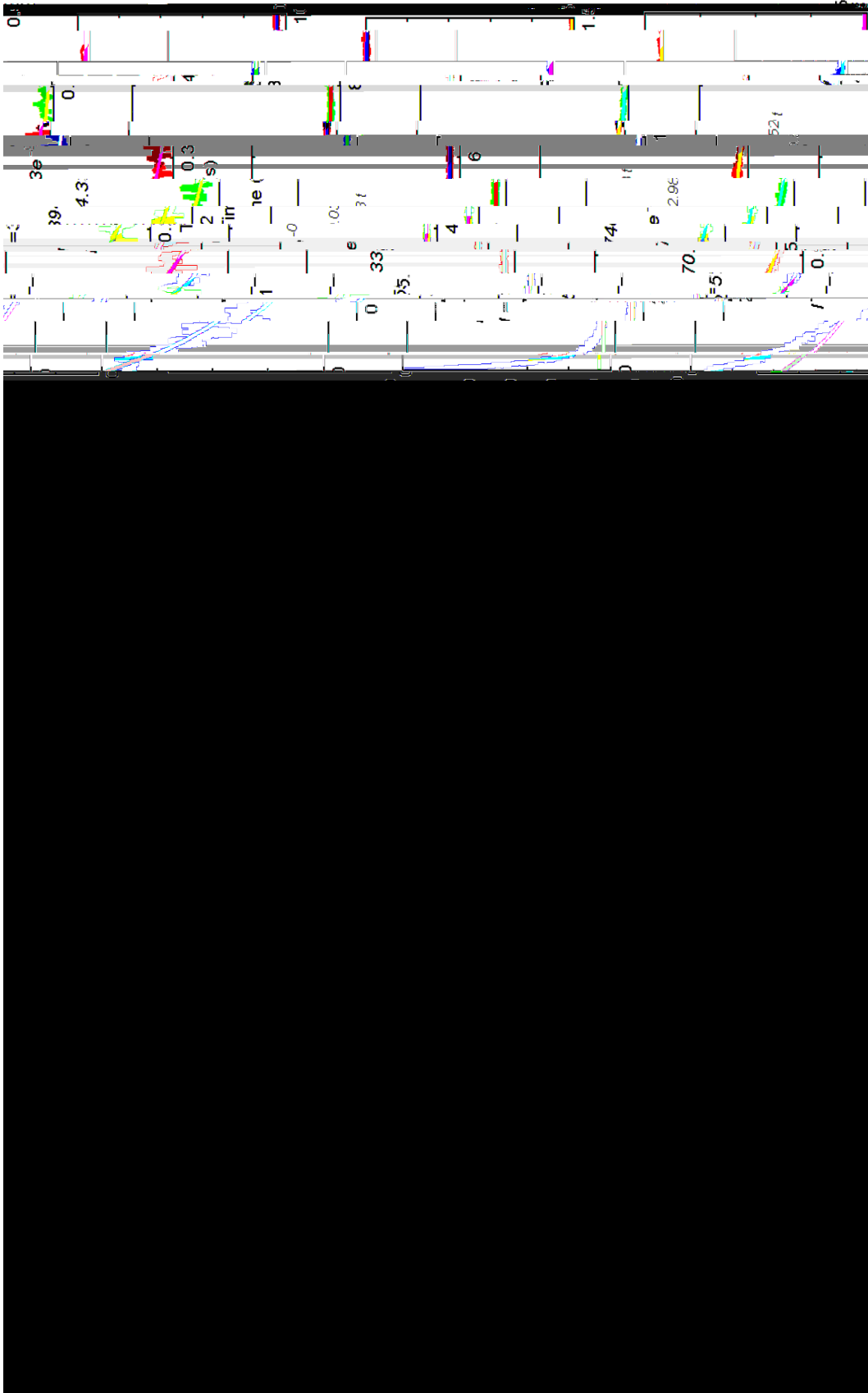


Figure 4.1 Peeling technique to get initial guess for Lev-Marq algorithm.

In conjunction with curve peeling algorithm the *Lev-Marq* method gave good result as seen in Table 4-1 and Figure 4.2. This table presents parameters of OSL component along with their confidence interval. The small range of confidence interval indicates that the value of isolated component may vary in this range.

Components	Amplitudes	Confidence interval (95%)	Decay Parameters	Confidence interval (95%)
1	80.7	(79.2, 82.3)	-2.184	(-2.240, -2.129)
2	11.7	(10.2, 13.2)	-0.444	(-0.498, -0.391)
3	7.4	(7.2, 7.6)	-0.004	(-0.005, -0.003)

Table 4-1 Parameters isolated using *Lev-Marq* method along with peeling technique. The OSL considered here corresponds to a pond sample (PARB TL1) and initial intensity was around 10000 units.



Figure 4.2 OSL decay modeled by sum of three exponentials.

4.4 Quality of fitting and validation of component

Fitting a model function to a set of experimental data involves minimization of χ^2 . The function truly represents the experimental data only when the data is randomly dispersed about it. Secondly, if the function comprises several components, it is important to objectively decide the number of terms to be retained in the fitting. This number should have a physical basis. Though the use of higher number of components in the model may provide lower χ^2 , the parameters thus obtained can be unphysical. For instance the physical interpretation of OSL model necessitates that decay parameter can not be positive and amplitudes can not be negative. However, the use of large number of component (exponentials) to OSL data may result into a few positive decay parameters and negative amplitudes which is unrealistic (Figure 4.4c and Figure 4.4d). Thus, estimation of an optimum number of components in the model is necessary for correct interpretation of experimental data. In view of this, the statistical tests such as analysis of residuals, chi-square test and F-test were carried out [9, 10].

4.4.1 Sensitivity of model parameters: A comparative study

$$I_1 = 3e^{-t} + 2e^{-2t} + 1e^{-3t}$$

$$I_2 = 3.156e^{-1.012t} + 2.875e^{-2.301t}$$

$$I_3 = 3.824e^{-1.064t} + 6.632e^{-3.592t} - 4e^{-6.360t}$$

Time (t)	I_1	I_2	I_3	Relative difference (%) $(I_2 - I_1)/I_1$
----------	-------	-------	-------	--

Here a and λ correspond to true value of model parameters while a^* and λ^* are obtained by changing a and λ by a small value h i.e. $a^* = a + h$ and $\lambda^* = \lambda + h$. The higher value of E for a particular parameter implies that the model function is very sensitive to it and small change in this parameter will cause a large change in value of function. Thus the sensitivity for particular model parameter is defined as

$$S(a_i) = \frac{E(a_i^*)}{E(a_i)} \quad (4.12)$$

$$S(\lambda_i) = \frac{E(\lambda_i^*)}{E(\lambda_i)} \quad (4.13)$$

To illustrate sensitivity of various model parameters, it was calculated according to the formulation proposed by Julius et al. [11] and sensitivity of parameters for a typical OSL is given in Table 4-3

Component	OSL parameters		Sensitivity of parameters	
	Amplitude (a_i)	Decay parameter (λ_i)	S (a_i)	S (λ_i)
1	81	-2.184	1.99	988.57
2	12	-0.444	7.61	2641.34
3	7	-0.004	214.81	5144851.85

Table 4-3 Sensitivity of various parameters of multiexponential model used for isolation of OSL components. The parameters used were obtained after isolating a typical OSL curve. $I(t) = 81e^{-2.184t} + 12e^{-0.444t} + 7e^{-0.004t}$. Here sampling interval was 0.16 s and total time was 40 s.

The value of S indicates the change in E that would result due to a small change in a particular parameter. For instance small change in decay parameter of component 1 (when λ changes to $\lambda + h$) will change the value of E by 1000 times its original value. That is, multiexponential model is more sensitive to exponents (decay parameters) rather th

makes isolation of components from OSL difficult when the data is either noisy or contains components whose parameters lie in close vicinity.

4.4.2 Analysis of residuals: Auto correlation

While fitting a model to data it is always possible that the same experimental data may be fitted well with two markedly different analytical expressions and may also give same approximate value of χ^2 . In such situations an incorrect choice of equation can be detected based on randomness of residuals. A suitable diagnostic tool for this is the autocorrelation function [12]. It provides a measure of cross correlation of data with itself and helps identify the repetitive patterns or trend in data. The autocorrelation function of the weighted residuals $C(t_j)$ for the present problem was defined as.

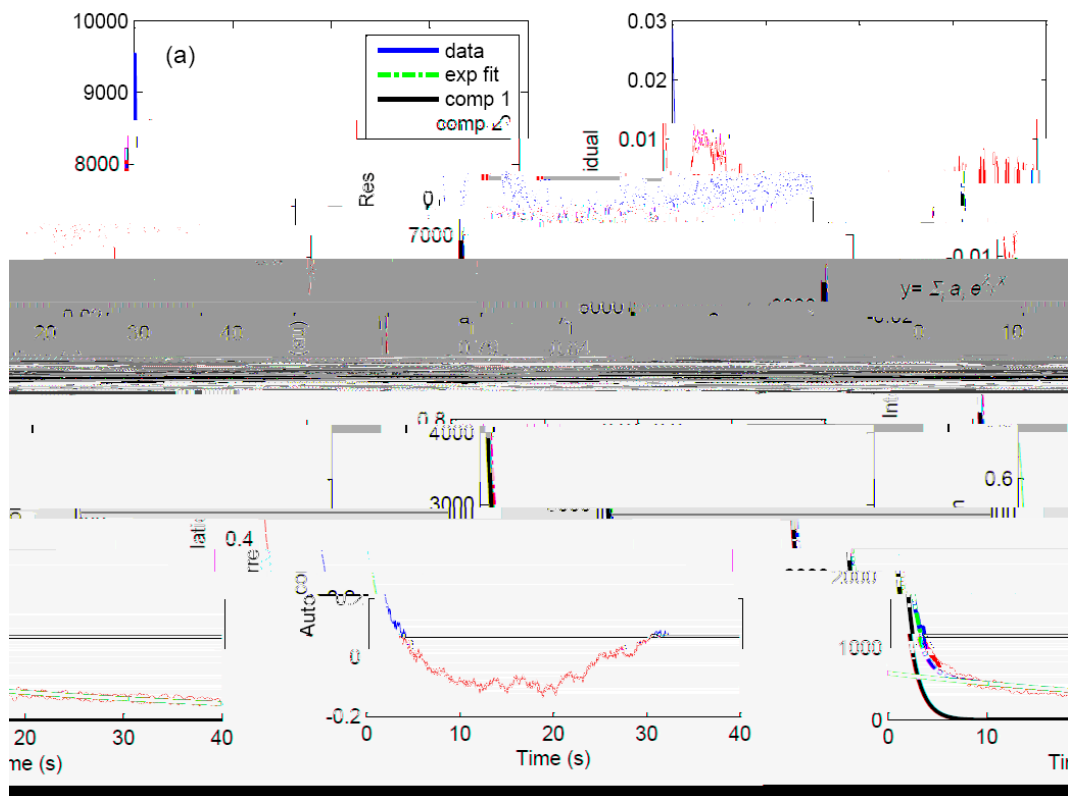
$$C(t_j) = \frac{\frac{1}{m} \sum_{i=1}^m w_i^{1/2} r(t_i) w_{i+j}^{1/2} r(t_{i+j})}{\frac{1}{n} \sum_{i=1}^n w_i r(t_i)^2} \quad j = 1, 2, \dots, n-m \quad (4.14)$$

where $r(t_i) = \hat{I}(t_i) - I(t_i)$, n is the number of time intervals for which experimental data is available, and m is the number of terms in the numerator. j can assume the values

to the weight assigned to each residual and it is defined as $w_i = I(t_i) / \sum \sqrt{I(t_i)}$.

$C(t_j)$ was evaluated for the values of j ranging from 0 to $n/2$, such that m is always greater than $n/2$. If the experimental data scatter randomly about model function $\hat{I}(t_i)$, and if m tends to infinity, $C(t_j)$ will become 0 for $j \neq 0$. In practice, due to the finite value of m , $C(t_j)$ when plotted as a function of time t_i is

Auto correlation analysis was used to verify the randomness of residuals and to establish the number of component. Figure 4.4 shows OSL fitted by the models containing successively higher number of terms. Clearly, three components provide an optimum fit. This is further supported by Figure 4.4 where the residuals are plotted as function of time. Four different models with different terms are examined. To assess the randomness of residues their autocorrelation was also plotted as function of time (Figure 4.4). Figure shows that the autocorrelation for residuals corresponding to models not containing three terms show a trend while for three terms, the autocorrelation show low amplitude and high frequency fluctuations.



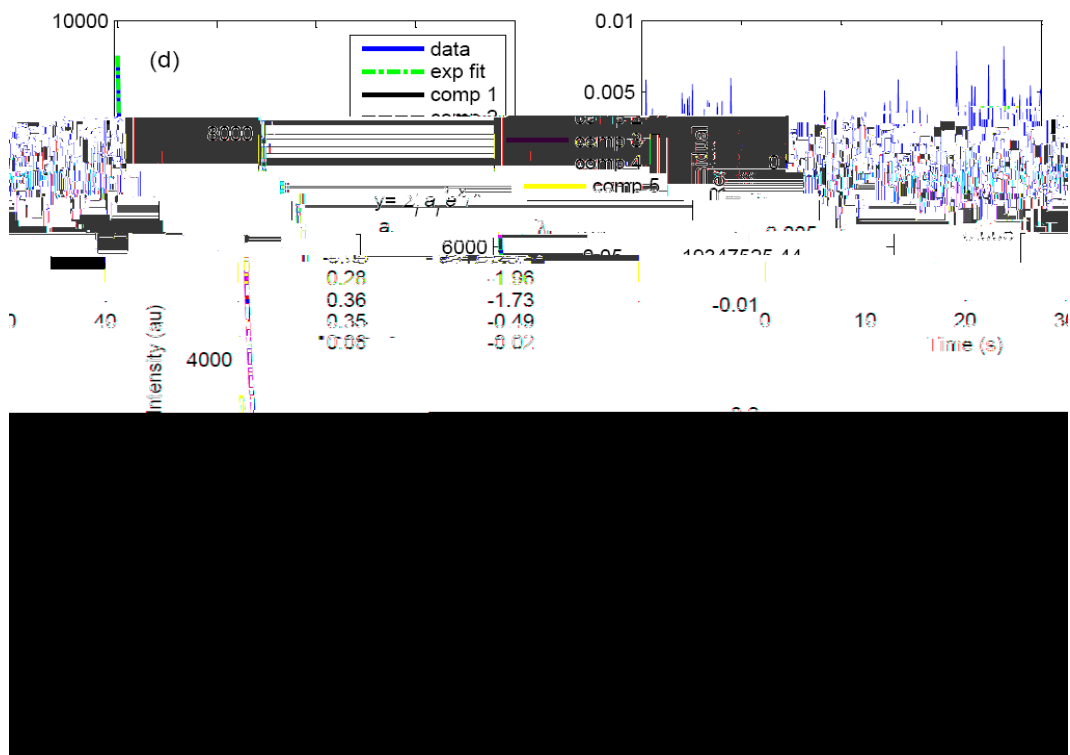


Figure 4.3 Autocorrelation test to monitor the randomness of residuals (a) two components fitted to data (b) three components fitted to data (c) four components fitted to data and (d) five components fitted to data.

4.4.3 Chi-Square test

For a normally distributed experimental data, it can be shown that the resulting χ^2 will follow χ^2 -distribution whose analytical form is given below.

$$f(\chi^2) = \frac{1}{2^{\nu/2} \Gamma(\nu/2)} e^{-\chi^2/2} (\chi^2)^{(\nu/2)-1} \quad (4.15)$$

The mean and variance of this distribution are ν and 2ν respectively. Here ν is degree of freedom and Γ is Gamma function. In present case if there are M parameters in model function and N OSL data points then the degree of freedom will be $N-M$. Now, the Median is the value of χ^2

In order to quantify the proximity of the experimental χ^2 distribution consider the integral defined below

$$Q = \int_{\chi_v^2}^{\infty} f(\chi^2) d\chi^2 \quad (4.16)$$

Here χ_v^2 is obtained from experimental data using expression (4.3) and Q represents the area of distribution between limits χ_v^2 and ∞ . Q is around 0.5 then the experimental χ^2 lies in close proximity to median of χ^2 distribution and hence the model represent

Q indicates that the experimental χ^2 is away from the median a Q approaching 1 implies that χ^2 is very low and indicates over fitting. In other words model

This Q parameter and χ^2 for various values of χ^2 are included in the table below. Q is seen and the value of Q approaches 1 suggesting redundant parameters in the model.

No of components	χ^2	Q	F_χ
1	3.16 e-1	0	-
2			5
3			7
4			-
5			4

T 4 a χ^2 , Q - a b n d F 4 l
T χ^2 d o e s n o t c h a n g e a

4.4.4 F-test

F-test helps in deciding the number of term in the model on the basis of χ^2 . If we fit a function with m terms to experimental data, the resulting value of χ^2 associated with the deviation about the regression $\chi^2(m)$ has $N - m$ degrees of freedom. If we add another term to the fitting function, the corresponding value of chi-square $\chi^2(m+1)$ has $N - m - 1$ degrees of freedom. The ratio of $\frac{\chi^2(m) - \chi^2(m+1)}{\chi^2(m+1)}$ forms a statistic F that follow the F distribution.

$$F = \frac{\chi^2(m) - \chi^2(m+1)}{\chi^2(m+1)/(N - m - 1)} = \frac{\Delta\chi^2}{\chi^2} \quad (4.17)$$

to calculate $\partial a_j / \partial I(t_i)$ at a point where χ^2 is minimum (in parameter space). In other words we want

$$\frac{\partial \chi^2}{\partial a_m} = 0 \quad (4.19)$$

Rewriting χ^2 defined in equation (4.3) in a more convenient form,

$$\chi^2 \equiv \sum_{i=1}^N \frac{\hat{I}(t_i; \hat{a}) - I(t_i)}{\sigma_i}^2 = \sum_{i=1}^N w_i \hat{I}(t_i; \hat{a}) - I(t_i)^2 \quad (4.20)$$

where $w_i = 1/\sigma_i^2$

From equations (4.21) and (4.22) we have

$$\frac{\partial \chi^2}{\partial a_m} = \sum_{i=1}^N 2w_i \hat{I}(t_i; \hat{a}) - I(t_i) \frac{\partial \hat{I}(t_i; \hat{a})}{\partial a_m} = 0 \quad (4.21)$$

The Jacobian of the model function $\hat{I}(t_i; \hat{a})$ with respect to set of parameters \hat{a} is defined as

$$J_{im} = \frac{\partial \hat{I}(t_i; \hat{a})}{\partial a_m} \quad (4.22)$$

Substituting equation (4.24) in equation (4.23) we have

$$\frac{\partial \chi^2}{\partial a_m} = \sum_{i=1}^N 2w_i \hat{I}(t_i; \hat{a}) - I(t_i) J_{im} = 0 \quad (4.23)$$

To find $\partial a_i / \partial y_j$, differentiate the above equation with respect to y_j .

$$\begin{aligned}
& \sum_{i=1}^N w_i \frac{\partial \hat{I}(t_i; \mathbf{a})}{\partial I(t_j)} - \frac{\partial I(t_i)}{\partial I(t_j)} J_{im} = 0 \\
& \Rightarrow \sum_{i=1}^N w_i \sum_{n=1}^m \frac{\partial \hat{I}(t_i; \mathbf{a})}{\partial a_n} \frac{\partial a_n}{\partial I(t_j)} - \frac{\partial I(t_i)}{\partial I(t_j)} J_{im} = 0 \\
& \Rightarrow \sum_{i=1}^N w_i \sum_{n=1}^m J_{in} \frac{\partial a_n}{\partial I(t_j)} - \delta_{ij} J_{im} = 0, \quad \delta_{ij} = \begin{cases} 1, & i = j \\ 0, & i \neq j \end{cases} \quad (4.24) \\
& \Rightarrow \sum_{i=1}^N w_i \sum_{n=1}^m J_{in} J_{im} \frac{\partial a_n}{\partial I(t_j)} = w_j J_{jm} \\
& \Rightarrow \sum_{n=1}^m \sum_{i=1}^N w_i J_{in} J_{im} \frac{\partial a_n}{\partial I(t_j)} = w_j J_{jm}
\end{aligned}$$

In above expression the term in the curly bracket represents Hessian matrix i.e.

$$H = \sum_{i=1}^N w_i J_{in} J_{im} \quad (4.25)$$

The equation (4.24) then reduces to

$$\sum_{i=1}^N H \frac{\partial a}{\partial I(t)} = w J \quad (4.26)$$

Solving equation (4.26) we have

$$\frac{\partial a_k}{\partial I(t_j)} = w_i \sum_{n=1}^m H_{kn}^{-1} J_{jn}, \quad \text{Where } k = 1, 2, \dots, m \quad (4.27)$$

Substituting equation (4.27) in equation (4.18) we have

$$\sigma_{ij}^2 = \frac{1}{jj}$$

Thus the diagonal element H_{jj}^{-1} of the inverse of Hessian matrix represent the uncertainty in the parameter a_j and the off diagonal elements H_{jk}^{-1} represents the

Here I_i^{reg} is the luminescence signal integrated over first n channels for a given regeneration dose, a_i^{reg} and λ_i

many more algorithm like genetic algorithm, Prony, Laplace-pade etc exist for fitting multiexponential model. In present case *Lev-Marq* method was found most efficient in retrieving the OSL components.

3. Normalization of data Normalization method and proper statistical weight are employed to avoid ill conditioning of the fitting method. In present case OSL was normalized with its highest intensity and all data points were assumed to have Poisson error.
4. Effect of Noise:

Reference

1. Bailey R. M., Smith B. W., and Rhodes E. J. (1997). "Partial bleaching and the decay form characteristics of quartz OSL". *Radiation Measurements* **27**

Chapter 5

Component Specific Study: Dating

Perspective

5.1 Introduction

The present chapter concerns methodological aspects and practical application of the components specific analysis of OSL decay. Here the effect of noise arising due to counting statistics on isolation of components has been studied and a method is proposed to minimize its adverse effects. Section 5.2 of this chapter briefly reviews the work done on OSL components. Section 5.3 discusses the relevance and physical significance of model parameters in context of OSL. In section 5.4 the dependence of decay parameters on radiation dose and stimulation power are examined. The findings of this method components. Section 5.5 discusses the methodology for isolation of component. This section discusses the methodology for synthetic OSL profiles and then these sections discuss the effect of noise on the isolation of components. This section illustrates the inadequacies of fitting algorithm when SNR is poor and a

method is proposed to isolate the components. Section 5.6 highlights the observations made on dose retrieval by different components and SAR. Section 5.7 addresses various problems of the method proposed in section 5.5. Finally Section 5.8 summarizes the results.

5.2 Review of earlier work

Optically stimulated luminescence (OSL) has emerged as a preferred technique for dating of sediments and extensive effort has been put in developing this technique. The key issue is in determining equivalent dose (D_e) of OSL measurements. The OSL from quartz is expressed by a sum of exponentials, each being representative of the trap with different detrapping or photoionisation cross section [1, 2]. Linearly Modulated OSL (LM-OSL) at times even seven components have been reported [3]. Rapid photo-bleach characteristic of the fast component makes it a logical choice for the estimation of paleodose even from those samples that have not seen enough sun light prior to its deposition.

Usually, the equivalent dose is estimated by multiple aliquot, single aliquot and single grain techniques. In these techniques, the background subtracted initial part of luminescence signal (typically for one second of stimulation) is used for dose estimation. This choice of time window ensures that the SNR is high and it has so far been assumed that the signal in this time window is dominated by the fast component [4, 5]. However, the assumption holds only for cases where contribution of fast component is greater than 70%-80% of total OSL signal (area under the decay curve) and the decay parameter of the fast component is significantly higher than other components. In cases where the contribution of the medium component is comparable to the fast component, the initial signal also contains a significant contribution of medium component. For such samples the conventional analysis leads to erroneous paleodose. Besides this, the components other than fast are not only relatively less sensitive to light but also have different thermal stability, dose responses and/or recuperation characteristics [3, 6, 7] and hence isolation of these components would avoid additional complications.

The usefulness of the components of OSL in different context has led to a feverish activity in this field [8-14]. Many numerical [6, 15] and experimental attempts have been made to isolate OSL components. While the fast component is used for De estimation of the partially beached sample, the slow component has been recommended for extending the dating age range because of its higher saturation limit ~1000 Gy [2]. Attempts have been made to isolate slow component by optical washing with 100 s of illumination at 160 °C or by heating up to 450 °C or 500 °C (thermal washing) of fast and medium component. Similarly, it has been suggested that it is possible to isolate the fast component using IR stimulation at elevated temperature [16]. However, these methods results in OSL with poor signal to noise ratio and reliable retrieval of components embedded in large background in its truest form is not possible. In addition to this, it is difficult to ensure a complete depletion of fast component at elevated temperature due to low energy of IR stimulation. Besides the experimental techniques, the components are also isolated numerically by fitting a multiexponential model to OSL decay curve [2].

Numerical isolation of component strongly depends on SNR. For poor SNR the curve fitting method either fails to isolate the components or often yields parameters with no physical significance. Fitting algorithm also fails in cases where the model involves a large number of parameters.

5.3 Relevance of OSL model parameters

Extensive research has been done towards understanding the origin of multi-exponential nature of OSL and it has been charges originating from the distinct trapping sites with characteristic mean life times [2]. Depending on the mean life time of the trapped charge, the resulting components of OSL are generally termed as fast, medium and slow. However, the component with exceptionally high decay rate is termed as ultra fast component. Mathematically, the OSL decay from quartz can be represented as

$$I_{OSL}(t) = \sum_{i=1}^n a_i e^{-\lambda_i t} \quad (5.1)$$

Where a_i are the initial OSL intensities and λ_i

The decay parameters were significantly depended on the stimulation power. Table 5.1 lists the values of OSL parameters for three different stimulation powers and it is apparent that the life time of fast component is lowest for highest stimulating power. However, the medium and slow components are less sensitive to the given stimulation power. The above observations make it imperative that for component specific analysis using fast component the stimulation power must remain constant during experiments.

Dose (Gy)	Fast component			Medium component			Slow component		
	Stimulation Power (%)			Stimulation Power (%)			Stimulation Power (%)		
	50	70	90	50	70	90	50	70	90
50	0.74 ±0.05	0.98 ±0.06	1.22 ±0.09	0.21 ±0.06	0.20 ±0.03	0.22 ±0.01	0.011 ±0.002	0.009 ±0.001	0.011 ±0.001
100	0.76 ±0.03	1.01 ±0.06	1.24 ±0.07	0.24 ±0.03	0.22 ±0.03	0.23 ±0.01	0.013 ±0.001	0.011 ±0.001	0.011 ±0.001
150	0.76 ±0.06	1.05 ±0.08	1.24 ±0.07	0.21 ±0.04	0.23 ±0.03	0.22 ±0.02	0.012 ±0.002	0.012 ±0.002	0.011 ±0.001

Table 5-1 Decay parameters of OSL components for different stimulation power error in data is standard deviation of 5 different disk

5.5 Numerical experiments on synthetic OSL profiles

When fitting a non-linear function to experimental data it is necessary that a stable and convergent fitting algorithm be used to determine component parameters. The noise in the data critically governs the convergence of fitting algorithm and thus decides the correctness of the retrieved parameters. In this regard, χ^2 test and autocorrelation function were used to validate OSL components. Redundant parameters are identified by F-test. In view of the role played by noise in isolation of the OSL components, the present section elaborately investigates low and high intensity synthetic OSL profiles.

5.5.1 Generation of synthetic OSL profile

OSL signal involves photon counting statistic

point. Assuming that the experimental OSL comprises sum of three exponentials, the synthetic OSL profile was generated with three known exponentials including background and Poisson error. It is important to mention that inclusion of Poisson

5.5.2 Observations on synthetic OSL profiles

Using the above formulation, about 200 distinct synthetic OSL profiles with known initial intensities ranging from 500 to 25000 units were generated. These were then used to examine the efficacy of the fitting algorithm. Figure 5.3 presents a statistical visualization of the dependence of the correctness of retrieved parameters on initial intensities. It is clear that for low intensity cases, each component has a large scatter. A colorbar beside the figure also shows poor χ^2 thereby indicating a poor fitting. The retrieved parameters for 200 distinct high intensity profiles are shown in Figure 5.3c and Figure 5.3d. It is apparent that there is negligible scatter in the retrieved parameters for each component. Besides this, the value of χ^2 for all 200 synthetic OSL profiles is considerably low thereby indicating an excellent fitting.

The spread in the values of parameter clearly indicates that it is impossible to retrieve correct components from low intensity OSL profiles. The convergence of fitting algorithm relies heavily on the number of parameters and sensitivity of parameter. This implies that if we remove the most sensitive parameter in model by putting constraints then isolation can be made even for low intensity OSL profile. In case of OSL, the decay parameters are most sensitive hence it is obvious that apriori knowledge of decay parameters would help a better isolation of components. In view of this following steps are proposed to isolate components from poorly SNR samples

1. Generate a high intensity OSL by giving a high dose to sample.
2. Isolate the components by *Lev-Marq* algorithm and get decay parameters and amplitudes of components.
3. Apply χ^2 test to check the quality of fitting and validate the number of components by F-test.
4. Use the decay parameters obtained in step 2 as fixed constants and isolate the OSL components from low intensity OSL profiles.

The rationale behind keeping decay rates constant is based on the reasonable observation that for a given stimulation power the decay rates remains invariant with respect to dose (Figure 5.1). The above approach was applied to low intensity synthetic OSL profiles with initial intensity of 500 and 1000 units. The effectiveness of the proposed algorithm is evident from the histograms in Figure 5.4 that shows a reduction in the spread of fast component amplitude. Also, the shape of histogram reduces to a well defined Gaussian. In order to compare the correctness and efficacy of proposed approach, the amplitudes of components from synthetic OSL profiles with intensities ranging form 500 to 20000 units were compared. Table 5-2 shows relative deviation (standard-deviation/mean) in the amplitudes of components.

Inten- sity	Amplitudes of Synthetic OSL decay curve								
	Known			Retrieved without fixing decay constant			Retrieved with fixing decay constant		
	Fast	Med	Slow	Fast	Med	Slow	Fast	Med	Slow
20000	14000	5000	1000	13956±258	4034±248	2038±317	13980±124	5009±56	1005±18
10000	7000	2500	500	6958±192	2042±182	1090±440	6996±92	2502±39	502±13
1000	700	250	50	653±116	248±113	118±84	700±35	250±17	50±8
500	350	125	25	271±90	175±94	53±37	350±25	125±13	25±7

Table 5-2 Comparison of amplitudes retrieved from synthetic OSL by proposed approach

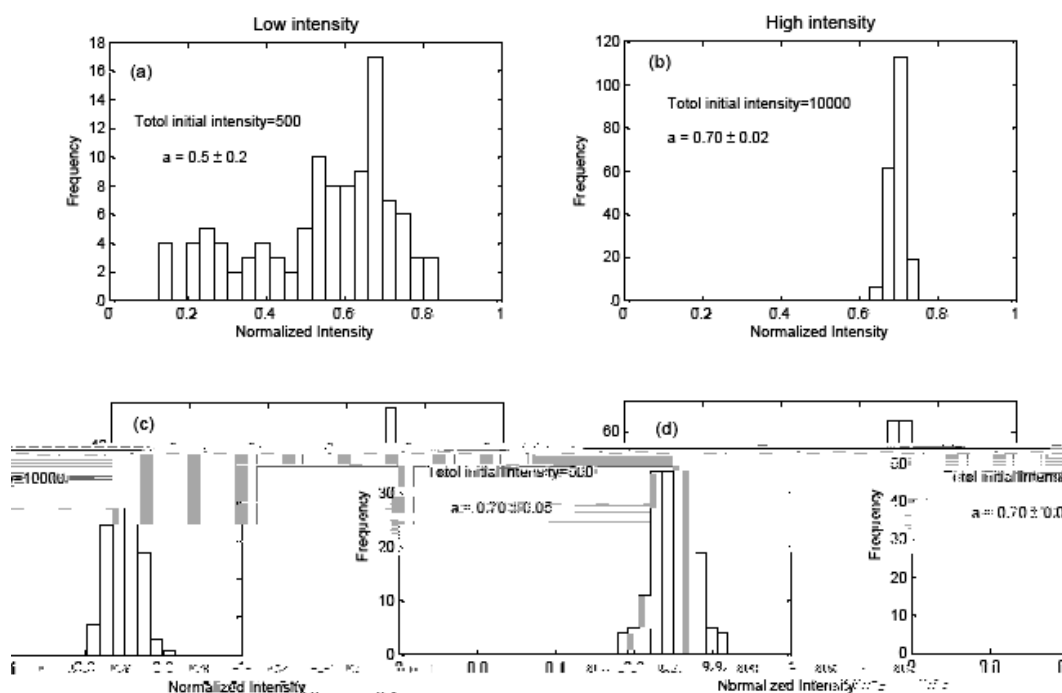


Figure 5.4 Comparison in spread of amplitudes of fast component retrieved by Lev-Marq algorithm (4a and 4c) and by proposed algorithm (4b and 4d). Upper two figure 4a and 4b shows comparison for low intensities while lower two figure 4c and 4d for high intensities.

For intensity of 500 units the relative deviation is much smaller than the relative deviation obtained without fixing the decay parameters (conventional approach). Thus these results suggest that by imposing constraints on the OSL decay parameters, a considerable improvement on the quality of fitting even for low SNR sample can be achieved. This proposed methodology will particularly be helpful in young and poorly sensitive samples.

5.6 Observations on dose retrieved from different components

The above approach was further tested by conducting dose recovery test, i.e. by retrieving a known laboratory dose administered to the sample. Figure 5.5 shows a growth curves for various components.

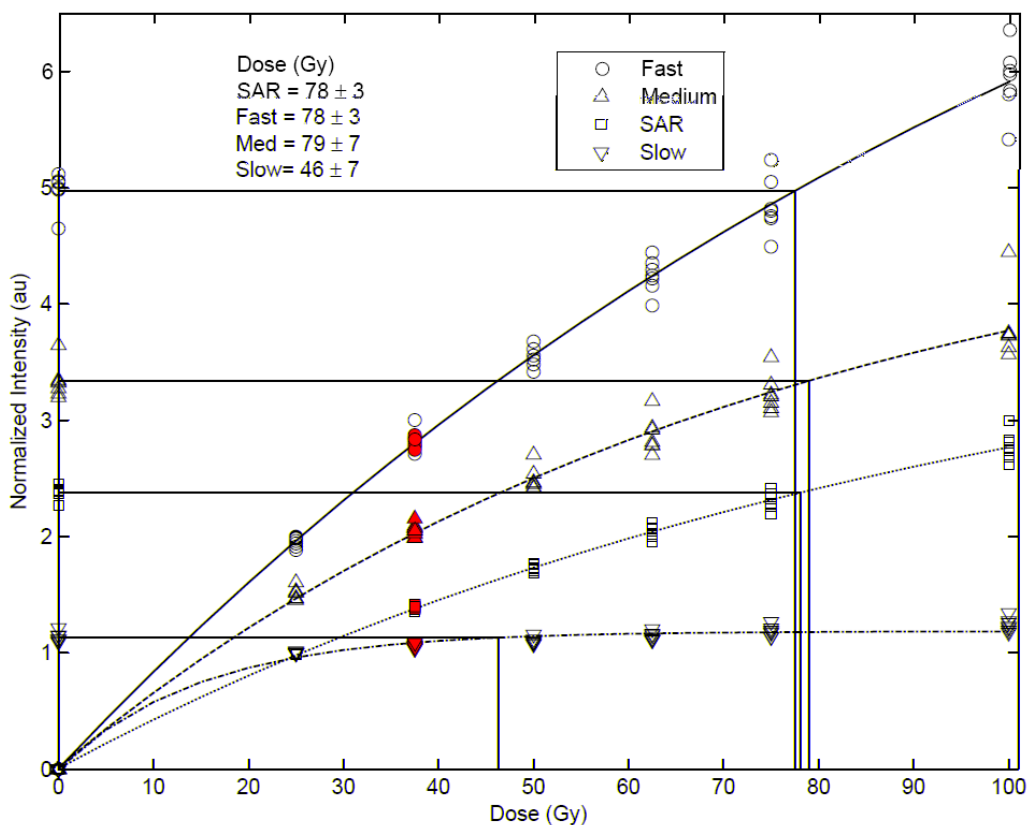


Figure 5.5 The growth curve for different components and SAR for seven disks where 75 Gy dose was given to sample

This figure shows that fast component is more sensitive to dose as compared to slow and medium. Curiously slow component saturated at low value of dose (~ 47 Gy) which contrasts to earlier observations. The saturated nature of slow component arises due to the fact that it can not be depleted in 40 s of optical stimulation [17].

Further to study the bleaching property of various components the sample was first given a dose of 75 Gy and then it was bleached with blue LED for varying time (0.2-2 s). Table enlists the values of doses computed using a standard SAR and using various components. Owing to the saturated nature and higher life time of slow component, it estimates a constant dose of 47 Gy for different illumination time (Table 5-3).

Illumination Time (Sec)	SAR (Gy)	Fast (Gy)	Med (Gy)	Slow (Gy)
0.0	78±3	77±2	78±2	48±7
0.4	54±4	46±1	64±6	46±5
0.8	43±3	35±1	54±8	49±7
1.2	36±3	29±1	49±9	47±7
2.0	31±3	25±1	40±9	48±5

Table 5-3 Comparison of doses estimated for different illumination time by different components and SAR. Here error is standard deviation of 5 disks.

As seen from table SAR and medium component always overestimate the dose while slow component shows a dose of 47 Gy irrespective of the illumination time. It can thus be inferred that fast component is readily bleached component as compare to medium and slow component.

5.7 Quantifying interference of components

The applicability of SAR protocol relies on assumption that the fastest decaying component of OSL dominates the initial part of OSL (typically of ~1sec). Considering the multiexponential decay of the OSL, it is obvious that this assumption would break down in cases where components other than fast component contribute comparatively. In such a situation the conventional SAR would provide erroneous result. The disparity between SAR and component specific analysis is further accentuate for partially bleached sample. The present section quantifies the error in application of standard SAR when the contribution of slow and medium components is considerable for a partially bleached sample. Towards this an analytic approach was followed to estimate the effect of medium and slow component in causing disparity between the doses estimated using SAR and the fast component. The expression for OSL comprising of three components is

$$I(t_k) = \sum_{i=1}^3 a_i e^{-\lambda_i k \Delta t} \quad (5.2)$$

Here $I(t_k)$ is the OSL intensity at time t_k (k^{th} channel) and Δt is the sampling interval at which OSL is recorded. Since in SAR dose is estimated by integrating OSL intensity of first few channel, the dose is given by

$$D \propto I$$

$$D_{SAR} = K_{SAR} \sum_{k=1}^n \sum_{i=1}^3 a_i e^{-\lambda_i k \Delta t} \quad (5.3)$$

Here n represents the number of channels over which intensity is integrated. K_{SAR} is constant of proportionality (Sensitivity of sample).

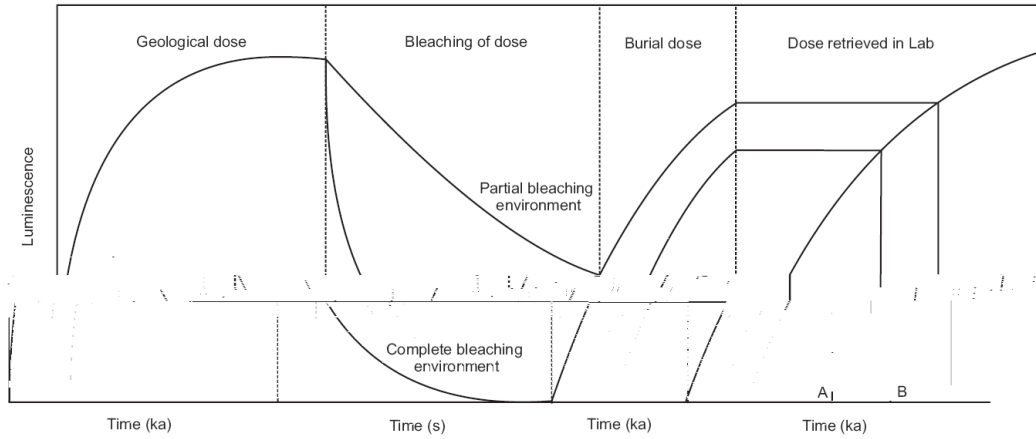


Figure 5.6 The events undergone by sediments prior to its deposition. The figure illustrate the development of signal at various stage

Figure 5.6 shows various events the sediment experiences prior to OSL measurement. As seen in figure the sediment has past geological dose. During transportation this dose gets bleached partially or completely due to day-light. And once again the dose starts building once the sample gets buried. Thus the total dose acquired by the sample is given as

$$Total\ dose(D_t) = Geological\ dose(D_g) - Bleached\ dose(D_{blc}) + Burial\ dose(D_{bur}) \quad (5.4)$$

$$D_t = (D_g - D_{blc}) + D_{bur} \quad (5.5)$$

In present case D_g is dose given to sample before it is bleached, D_{blc} corresponds to the dose that has been removed from the sample due to exposure to blue LED

and D_{bur} is the dose given to sample after it has been bleached. From equations(5.2), (5.3) and (5.5) the dose can be now rewritten as

$$D = K_{SAR} \sum_{k=1}^n \sum_{i=1}^3 a_i^{D_g, D_{blc}, D_{bur}} e^{-\lambda_i k \Delta t} \quad (5.6)$$

$$\frac{D_{SAR} - D_{bur}}{D} = \frac{\sum_{i=1}^3 a_i^{D_s} e^{-\lambda_i t_b} c_i}{\sum_{i=1}^3 a_{bur}^{D_{bur}} c_i} \times 100 \% \quad (5.11)$$

$$\frac{D - D_{bur}}{D} = \frac{a_1^s e^{-\lambda_1 t_b}}{a_1^{bur}} \times 100 \% \quad (5.12)$$

The above expression implies that the deviations in the dose estimated by SAR depends on the bleaching time, burial dose, geological dose and the contribution of various components to OSL. In this investigation the parameters were varied appropriately and the deviation of the doses estimated by SAR and fast components were calculated using expressions (5.11) and

$$a_i^{D_{bur}} \text{ and } a_i^s$$

total OSL

($\lambda_1 = \lambda_2 = \lambda_3 =$). Bleaching involved is essentially equivalent to that due to Blue Led stimulation.

The effect of medium component on overestimation of dose by SAR is given in Table component increases from 5 to 85% of total OSL, the deviation of dose estimated by SAR from the true dose increases from 38 to 46% even for integration of a few second (first five channels) of OSL. However the fast component deviates from the true dose only by 0.02%. These observations indicate that the assumption of dominance of fast component in the first few sec of OSL is only valid if contribution of medium component is very low. Thus SAR protocols estimates the dose correctly only if the contribution of medium component to OSL is negligible as compared to that of fast.

Bleaching time	Fast comp contribution (%)	Medium comp contribution (%)	Deviation in dose by SAR (%)	Deviation in dose by Fast (%)
5	10	85	46.3	0.02
5	20	75	45.5	0.02
5	30	65	44.6	0.02
5	40	55	43.7	0.02
5	50	45	42.7	0.02
5	60	35	41.6	0.02
5	70	25	40.5	0.02
5	80	15	39.3	0.02
5	90	05	37.9	0.02

Table 5-4 Deviation in doses estimated by SAR and fast component for bleaching of 5s which equivalent to 10 mean life of fast component. Here the decay parameters of fast, medium and slow were 2.2, 0.44 and 0.04 respectively. The contribution of medium component was varied from 5 to 85%

Besides the interference of medium component, SAR protocol is greatly affected by the geological dose. If the burial dose is very small as compared to the geological dose the SAR will always overestimate for partially bleached samples. To quantify this overestimation for various burial doses, the burial dose was varied from 10 to 90 % of geological dose for different bleaching times. Table 5-5 presents the deviation in dose estimated by SAR and fast component from the true dose for various values of burial dose and for various bleaching times.

Burial-dose(% of Geol dose)	Deviation from burial dose $\frac{D_{SAR, Fast} - D_{bur}}{D_{bur}} \times 100 \%$					
	Bleaching = 1sec		Bleaching = 3sec		Bleaching = 5sec	
	SAR	Fast	SAR	Fast	SAR	Fast
10	322.0	135.33	118.93	2.48	81.03	0.05
20	161.01	67.67	59.47	1.24	40.51	0.02
30	107.33	45.11	39.64	0.83	27.01	0.02

and fast component is 81 and 0.05 % respectively when burial dose is 10 % of geological dose. However if the burial dose is increased to 90% of the geological dose, then deviation in SAR reduces to 9%. This result shows that SAR is consistent only for the case where the burial dose is comparative to the geological dose. In view of this, it is likely that SAR overestimates the dose of the younger samples and hence is advisable to use fast component for such samples.

The conclusions of the analytic approach were corroborated by the findings of an experiment on a laboratory bleached sample. Towards this, OSL measurements on a sensitive quartz sample (PARB) were carried using Riso TL/OSL reader, [18]. UV window, blue stimulation and thermal assistance of 125°C are used. Single aliquot regenerative (SAR) protocol [19] was followed for dose estimation. The OSL signal was sampled at time resolution of 0.16 sec to reduce the discreteness of data. This minimum time resolution ensured the isolation of different OSL component.

To simulate the partial bleaching and subsequent accumulation of dose by sample, a completely bleached sample was given a dose of 1000 Gy. This sample was then bleached for different time duration (1 to 5 sec). The bleaching time here corresponds to the sun bleaching during the transportation of the sediment. After bleaching, a dose of 50 Gy was administered to the sample akin to the dose acquired by the partially bleached sample after its burial. The dose given to the sample was then recovered using fast and SAR.

Table 5-6 presents the dose estimated using SAR and OSL components for

amamipa lengwits of i7-csu

5.8 Case studies

5.8.1 Paleodose of partially bleached sediment: Tsunami sediment

The devastating tsunami of Dec 26, 2004 in south east Asia was triggered by a seismic moment magnitude (Mw) 9.1 earthquake [20] with epicenter near Banda Aceh, Sumatra. Geological records of geodynamic processes leading to such earthquakes suggest that the south pac

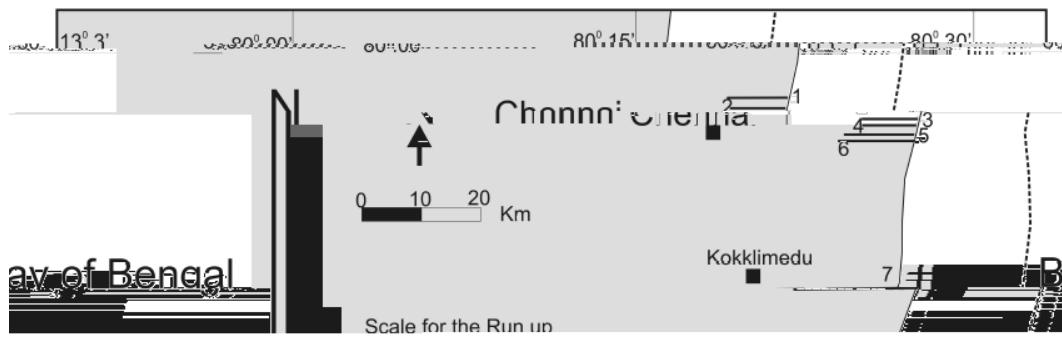


Figure 5.8 Coastal area and the sampling localities (1-9). Horizontal lines indicate the run-up elevation. Dotted line indicates the 100 m depth contour.

Analysis and interpretation of paleodoses

The paleodose from SAR on eight samples varied between 0.53 ± 0.01 to 0.78 ± 0.01 Gy. The mean fast component paleodose varied from 0.5 ± 0.2 to 0.7 ± 0.1 Gy. The Table 5-7 summarize the luminescence data and Figure 5.9 provides typical dose distributions using SAR and by using fast component.

Site No.	Locality	Sample code	No. of Disk	Dose rate (Gy/ka)	Dose (SAR)	Mean Dose (Fast-Comp)	Least 10% (Fast-Comp)
1	Coovum River mouth	CVR	20	1.9 ± 0.1	0.55 ± 0.01	0.5 ± 0.2	0.20 ± 0.03
2	Marina Beach	MGR	25	2.5 ± 0.1	0.65 ± 0.01	0.5 ± 0.2	0.1 ± 0.1
3	Sreenivasapuram	SNP	25	2.2 ± 0.1	0.69 ± 0.01	0.6 ± 0.2	0.37 ± 0.05
4	Foreshore Estate	FRS	25	1.7 ± 0.1	0.57 ± 0.01	0.5 ± 0.1	0.09 ± 0.04
5	Pattinapakkam	PTM	25	1.7 ± 0.1	0.70 ± 0.01	0.6 ± 0.2	0.27 ± 0.05
6	Eliot's Beach	EB	25	2.0 ± 0.1	0.63 ± 0.01	0.6 ± 0.2	0.04 ± 0.03
7	Kokklimedu	MKN	20	2.4 ± 0.2	0.53 ± 0.01	0.5 ± 0.2	0.02 ± 0.03
8	Porto Nova	NGP	25	2.6 ± 0.2	0.78 ± 0.01	0.7 ± 0.1	0.56 ± 0.02
9	Pichavaram	PCN	20	1.7 ± 0.1	0.53 ± 0.01	0.5 ± 0.2	0.02 ± 0.03

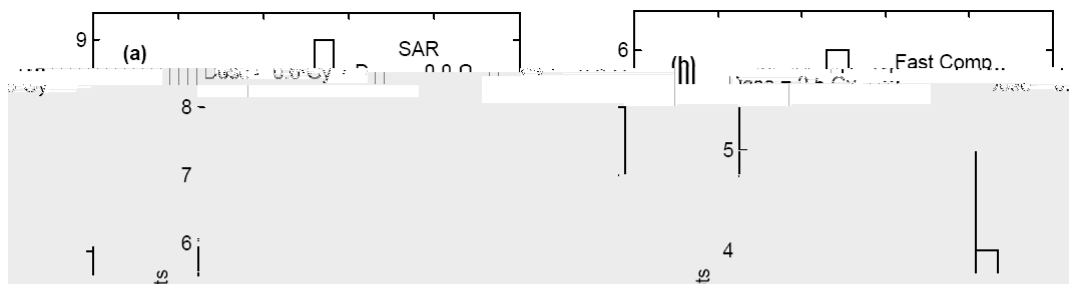


Figure 54 (a) Distribution of paleodoses measured using the SAR protocol. (b) Paleodose distribution using fast component of the OSL decay.

The consistency in the paleodoses from the conventional SAR and the fast component SAR suggests that the samples were well bleached before deposition during the Tsunami. In a short lived, high energy sediment transport event, durations over which the day light exposure is limited, partial bleaching of sediment during transportation is unlikely. The consistency of the OSL paleodoses, therefore suggest that the tsunami picked up only the near surface sands residing in the sediment-water interface region of the intertidal zone, transported them landwards and deposited them, (Figure 5.10).

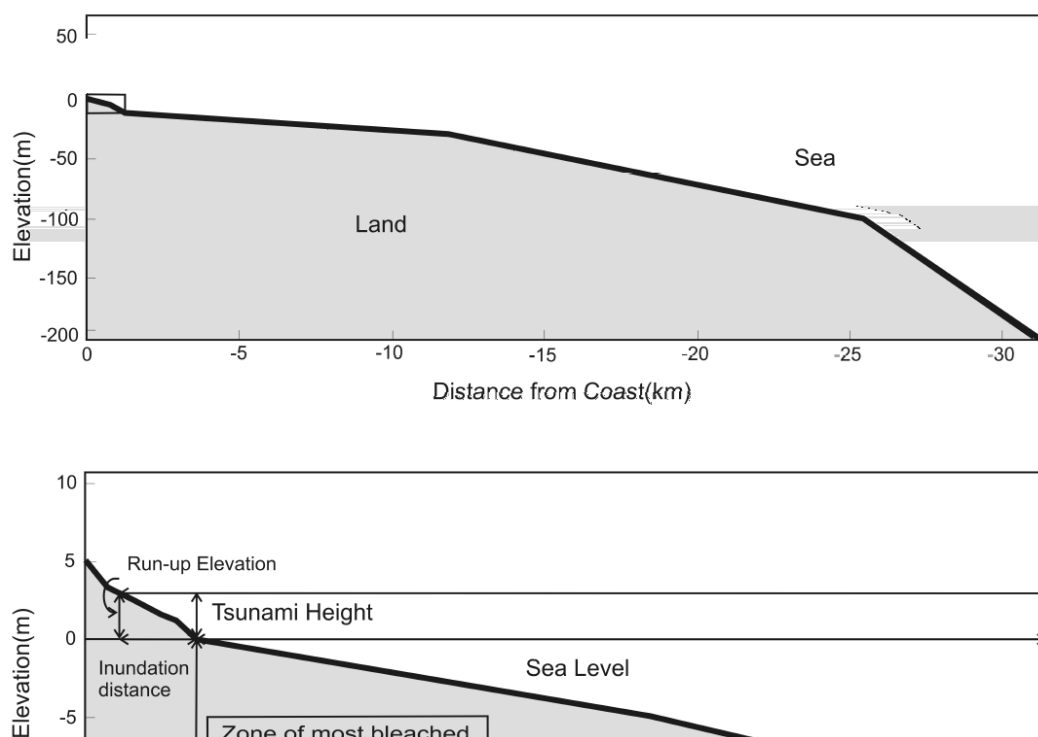


Figure 5.10 (a) Approximate bathymetry of the region. (b) Approximate bathymetry of the coast near Nagapattinam. The zone of most bleached sediments comprises sediments up to a depth of 10 m and in the intertidal zone.

In the tidal regions, constant reworking of sediments ensures that they are exposed to daylight, which bleaches their OSL to a low, near constant residual value. In these regions, sediment stratification also occurs and published results on sediment cores from tidal zone indicate young ages. These surface are immediately followed by ages of ~1ka or more [23, 24]. ^{14}C ages from the study area also show an abrupt increase of age with depth. For example, at Mammallapuram, sample AA30024 from a depth 45-50 cm, yielded a ^{14}C age of 1620 ± 110 a BP. Similarly sample BS 1608 from Marakkanam, near Pondicherry at depth 86-88cm yielded a ^{14}C age of 1563 ± 130 a BP [25]. If the tsunami had excavated older layers of tidal region, then due to the possibility of limited bleaching during a tsunami transport, a larger scatter in the paleodose distribution of modern tsunami should have been seen (due to a mixing up of upper bleached and lower older sample with higher paleodose). Thus a

narrow dose distribution in samples, laterally spread over 200 km indicates that no admixture from beach dunes or deep sediment layers under water (> 50 cm) occurred.

Given that the present tsunami was one of the most energetic events ever, the narrow paleodose distribution suggests that despite their ferocious energetic, in tsunamis in general can rework only the top ~50 cm or less, of the intertidal region. An indirect implication of this is the estimation of an upper bound to the sediment flux that can be transported by a tsunami event. This is a useful input to the sediment flux estimation for various inundations scenarios and is easily tested using Figure 5.11 and by earlier studies.

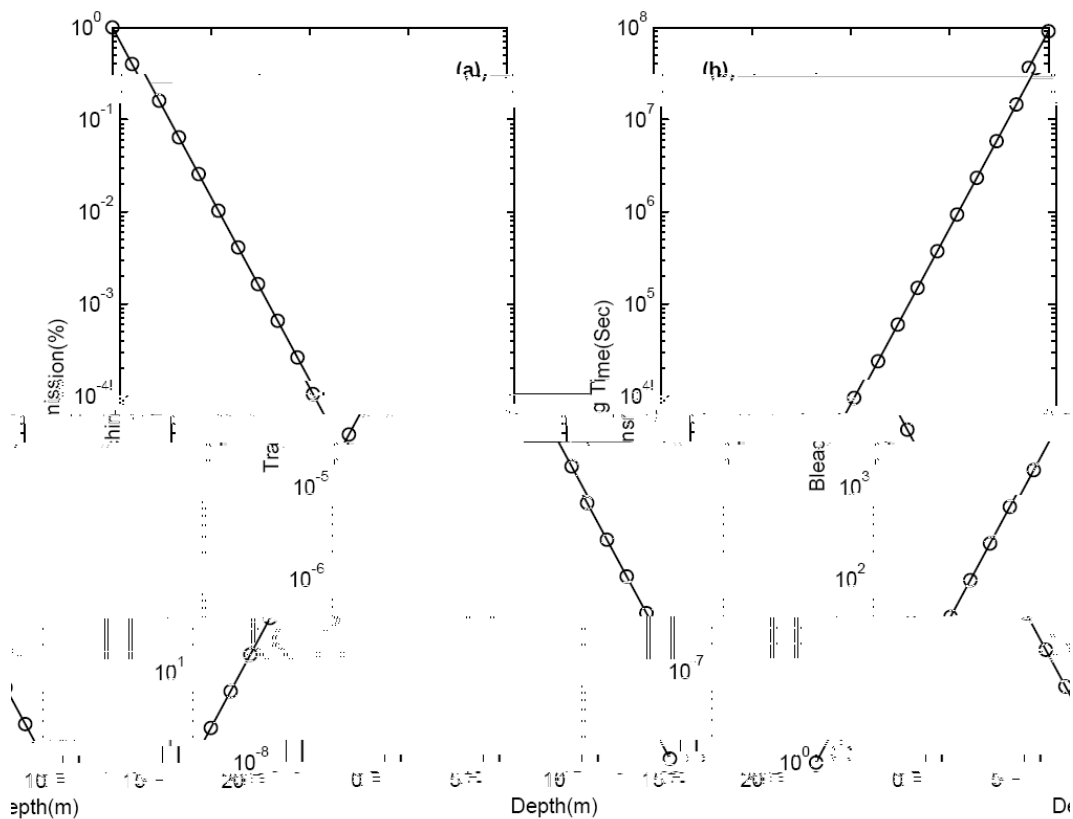


Figure 5.11 (a) Transmission of light in coastal water with high turbidity. Notice that the transmission spans eight orders of magnitude. (b) Bleaching time required for a 50% reduction of OSL signal at various depths based on data provided by Aitken and Jerlove [26, 27].

[28] observed that, i) daylight intensities at 4 m depth in a turbulent river waters were about 10^4 times lower than those at the surface, and ii) the daylight spectrum was severely attenuated below 500 nm and above 690 nm. Attenuation factors for 500 nm light of for high turbidity coastal water by Jerlov [27] and Smith [29] are given in Figure 5.11. For this case, only ~1% of light of wavelength 500 nm is transmitted to a depth of 5 m. Assuming a proportional reduction in bleaching, it would takes about 3 years at 20 m depth for highest turbid coastal water to get 50% reduction in signal. The depth of the sediment underwater is given in Figure 5.10 and if 10m is taken as a working limit where bleaching could proceed satisfactorily, then it is clear that only the sediments, that occur within a coast normal distance of a ~1km, should have seen daylight. This implies that for a meter along the coast line, the amount of sediment that can be potentially transported, will be the surface sediment lying in the 1 km coast-normal region would then be 500 m^3 [$1000\text{m} \times 0.5\text{m}$ (maximum depth to which bleached sediment resides) $\times 1\text{m}$]. This is similar to the measured sediment thicknesses [30]. This estimate can be refined further to a higher precision by measuring the OSL of samples from cores underwater and determining 1) the depth distribution of paleodose and 2) by measuring the suspended sediment load and their OSL level.

5.8.2 Study of components of quartz from different sites

A number of samples were analyzed and the parameters of isolated components are listed in the Table 5.8 three different sites.

Sample Name	Intensity	Fast Component		Medium Component		Slow Component	
		a ₁	λ ₁	a ₂	λ ₂	a ₃	λ ₃
Madurai (Tamilnadu, India)							
PARB TL-1	22780	80.7	-2.18	11.7	-0.44	7.4	-0.004
PARB TL-2	20098	80.5	-2.24	14.4	-0.65	4.4	-0.004
PARB TL-3	18137	79.0	-2.15	14.5	-0.50	5.6	-0.005
PARB TL-4	19149	72.0	-2.16	18.4	-0.53	9.7	-0.005
PARB TL-5	21231	78.8	-2.19	17.4	-0.62	3.2	-0.009
PARB TL-6	25038	70.8	-2.29	21.8	-0.63	6.2	-0.005
PAR/ TL-1	21781	76.8	-2.26	17.0	-0.53	5.6	-0.005
Morava River (Czech)							
Czech-Sec 3c-1	18132	46.3	-1.60	47.6	-0.53	4.6	-0.042
Czech-Sec 3c-4	24405	66.0	-1.33	32.9	-0.65	1.1	-0.017
Czech-Sec 3c-8	14862	60.9	-1.60	31.9	-0.63	5.6	-0.014
Czech-Sec 2-3	16590	55.2	-1.38	35.1	-0.33	8.1	-0.035
OB1	15779	53.0	-1.54	44.6	-0.65	2.5	-0.024
Tsunami 2004 (Tamilnadu , India)							
FRS	18444	69.2	-2.370	28.0	-1.140	2.9	-0.004
MGR	14296	78.7	-2.170	17.7	-0.720	3.8	-0.001
NGP	17200	41.6	-2.280	53.8	-0.880	4.6	-0.006
PTM	16052	84.4	-2.140	13.3	-0.840	2.3	-0.003

Table 5-8 Values of model parameters of different OSL components of various sample from three different sites.

In this study the behavior of different component was considered to examine the possibility of identifying any correlation between decay rates of OSL component and the ambient conditions. In this regard the components of quartz was examined to 1) Determine the number of parameters in quartz of different sources 2) determine the total range of their variations 3) examine possible use of the components for provenance studies. The component specific analysis of various sample showed the presence of three components viz. fast, medium and slow. The variation in decay parameters of different components for a given sample from a particular site was found negligible however, there was ~20% variation for sample from different sites (1.5 s^{-1} to 2 s^{-1}) (Table 5-9). This hints towards the fact that the quartz belonging to a particular origin may have specific decay parameters.

Sample	Location	Fast component (λ_1)	Medium component (λ_2)	Slow component (λ_3)
Mexico GD03-06	Desert (USA)	-2.21	-0.56	-0.007
Oman	Desert (Arabia)	-2.01	-0.51	-0.009
Maut 6-7	Desert (Libya)	-1.98	-0.49	-0.004
Pradip TL1-TL2	Desert (USA)	-1.72	-0.62	-0.008
PARB-TL1	Fluvial (Tamilnadu, India)	-2.13	-0.42	-0.004
Mahi DJ1	Eolin (South-Thar, India)	-1.50	-0.52	-0.030
Egypt	Desert (Egypt)	-1.51	-0.34	-0.030
Sant GPR-05	Desert (South Thar,India)	-1.39	-0.31	-0.014

Table 5-9 Decay parameters of OSL components of quartz from eight different sites

The distribution of traps in quartz reflects the geochemical environment at the time of formation and subsequent optical and thermal cycle experience by the sample from which it was collected. To unravel the connection between the decay rates of the components and the environmental condition experienced by quartz, we studied eight sensitive samples from different sites. Details of sites are given in Table 5-10

Sample	Location	Surrondings	Type of Rock
Mxico GD03-06	Desert (USA)	Great Basin, Mojave and Volcaninism	-----
Oman	Desert (Arabia)	OMAN mountains whose exposed surface formed largely by ophiolites and Permian to Cretaceous limestone and minor but distinctive radiolarian chert.	Aeolian sands, called aeolianite or miliolite which are derived from the biologically productive coastal zone. They are carbonate rich and consist of fragments of algae, frominifera, peloids, and shell fragments
Maut 6-7	Desert (W. Africa, Libya)	-----	-----
Pradip TL1-TL2	Desert (USA)	-----	-----
PARB-TL2	Fluvial (India)	Tamilnadu, Madurai,(India)	Granite
Mahi DJ1	Eolin (south Thar, India)	The aravalli hills demarcate the easternmost boundary of the desert	Rhyolite, granite, gneisses and quartzite
Sant GPR-05	Desert (South Thar,India)	The aravalli hills demarcate the easternmost boundary of the desert	Rhyolite, granite, gneisses and quartzite
Egypt	Desert (Egypt)	-----	-----

Table 5-10 Details of sites from where sample was collected

feldspar was found to have decay rate of about $\sim 0.8 \text{ s}^{-1}$ while that of quartz was around $\sim 2 \text{ s}^{-1}$ (Figure 5.12). Figure shows that the fast component of quartz could be resolved from the OSL of the mixture containing 30% feldspar by weight. As fast component of composite sample represents the fast components of quartz hence even for feldspar contaminated sample one can minimize the undesirable effects of feldspar.

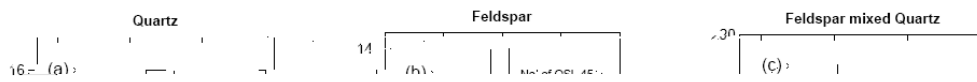


Figure 5.12 The histograms of decay rates from pure quartz, pure feldspar and quartz contaminated by 30% feldspar by weight.

5.9 Conclusions

In present studies methodological aspects and useful implications of component specific analysis have been dealt with. Isolation of components from OSL with poor signal to noise ratio is of main concern here. The outcomes of this chapter are enlisted below

1. OSL decay parameters are independent of dose and vary with stimulation power
2. Isolation of OSL component is possible even for OSL intensity of 500 units by proposed method with the help of numerical experiments on synthetic OSL profiles.
3. An analytical approach of studying interference of medium component shows that even 5% contribution of medium component to OSL can give overestimation in age.
4. An experiment conducted on laboratory made partially bleached sample shows that paleodose estimated using SAR always exceeded the value estimated by fast component specific analysis.
5. With component specific OSL dating technique, it is possible to date tsunami events with a reasonable accuracy. It is also possible to use luminescence dating to provide constraints on sediment influx during such events.
6. Fast component analysis can solve the problem of contamination of feldspar in sample as fast component of quartz can be resolved from the OSL of the mixture containing 30% feldspar by weight
7. Slow component saturates at low value of doses as compared to fast and medium which is against the earlier observation on slow components
8. Component study of various quartz from different origin shows variation if component but it is not conclusive

References

1. Smith B. W. and Rhodes E. J. (1994). "Charge movements in quartz and their relevance to optical dating". *Radiation Measurements* **23**(2-3): pp 329-333.
2. Bailey R. M., Smith B. W., and Rhodes E. J. (1997). "Partial bleaching and the decay form characteristics of quartz OSL". *Radiation Measurements* **27**(2): pp 123-136.
3. Jain M., Murray A. S., and Bøtter-Jensen L. (2003). "Characterisation of blue-light stimulated luminescence components in different quartz samples: implications for dose measurement". *Radiation Measurements* **37**(4-5): pp 441-449.
4. Murray A. S. and Wintle A. G. (2000). "Luminescence dating of quartz using an improved single-aliquot regenerative-dose protocol". *Radiation Measurements* **32**(1): pp 57-73.
5. Murray A. S. and Olley J. M. (2002). "Precision and accuracy in the optically stimulated luminescence dating of sedimentary quartz: a status review". *Geochronometria* **2**pp 11-16.
6. Singarayer J. S. and Bailey R. M. (2003). "Further investigations of the quartz optically stimulated luminescence components using linear modulation". *Radiation Measurements* **37**(4-5): pp 451-458.
7. Singarayer J. S. and Bailey R. M. (2004). "Component-resolved bleaching spectra of quartz optically stimulated luminescence: preliminary results and implications for dating". *Radiation Measurements* **38**(1): pp 111-118.
8. Murari M. K., Achyuthan H., and Singhvi A. K. (2007). "Luminescence studies on the sediments laid down by the December 2004 tsunami event: Prospects for the dating of palaeo tsunamis and for the estimation of sediment fluxes". *Current Science* **92**(3): pp 367-371.
9. Kiyak N. G., Polymeris G. S., and Kitis G. (2007). "Component resolved OSL dose response and sensitization of various sedimentary quartz samples". *Radiation Measurements* **42**(2): pp 144-155.
10. Chithambo M. L., Preusser F., Ramseyer K., and Ogundare F. O. (2007). "Time-resolved luminescence of low sensitivity quartz from crystalline rocks". *Radiation Measurements* **42**(2): pp 205-212.
11. Li S.-H. and Li B. (2006). "Dose measurement using the fast component of LM-OSL signals from quartz". *Radiation Measurements* **41**(5): pp 534-541.
12. Li B. and Li S.-H. (2006). "Comparison of De estimates using the fast component and the medium component of quartz OSL". *Radiation Measurements* **41**: pp 125-136.

13. Li B., Li S.-H., and Wintle A. G. (2006). "Observations of thermal transfer and the slow component of OSL signals from quartz". *Radiation Measurements* **41**(6): pp 639-648.
14. Bailey R. M. and Arnold L. J. (2006). "Statistical modelling of single grain quartz De distributions and an assessment of procedures for estimating burial dose". *Quaternary Science Reviews* **25**(19-20): pp 2475-2502.
15. Bluszcz A. and Adamiec G. (2006). "Application of differential evolution to fitting OSL decay curves". *Radiation Measurements* **41**(7-8): pp 886-891.
16. Jain M., Murray A. S., Bøtter-Jensen L., and Wintle A. G. (2005). "A single-aliquot regenerative-dose method based on IR bleaching of the fast OSL component in quartz". *Radiation Measurements* **39**(3): pp 309-318.
17. Bailey R. M. (2000). "The slow component of quartz optically stimulated luminescence". *Radiation Measurements* **32**(3): pp 233-246.
18. Bøtter-Jensen L., Bulur E., Duller G. A. T., and Murray A. S. (2000). "Advances in luminescence instrument systems". *Radiation Measurements* **32**(5-6): pp 523-528.
19. Wintle A. G. and Murray A. S. (2006). "A review of quartz optically stimulated luminescence characteristics and their relevance in single-aliquot regeneration dating protocols". *Radiation Measurements* **41**(4): pp 369-391.
20. Lay T., Kanamori H., Ammon C. [tD\(41Tf3l\)45H82dw 2.0b-dM\(A\)Nw 2A2\(e\)5\(91\)-5\(tD\(41143l\)452.9916 Tw](https://doi.org/10.1016/j.tdg.2016.05.001)

Chapter 6

Summary and future outlook

6.1 Summary

The methodological aspects of component specific analysis (CSA) and its applicability to samples of different kinds formed the central theme of the present work. The advantages of component specific analysis over the conventional SAR protocol have been dealt with in greater detail. The major results of the present investigations are briefly summarized below.

- The *Lev-Marq* algorithm was shown to be effective in retrieving the OSL components when OSL signal to noise ratio is high. It is demonstrated that for convergence of the algorithm to the true values of OSL parameters, the initial guess for the parameters to be fed to the algorithm should be chosen logically. In this regard the curve peeling technique was found successful and was incorporated in the *Lev-Marq* algorithm to isolate the OSL components. Further, the usage of various statistical tests viz. chi-square test, F-test, and analysis of residuals helped validate the OSL components.
- Numerical experiments on synthetic OSL profile have shown that the convergence of the *Lev-Marq* algorithm is critically governed by the SNR.

In the multiexponential model that describes the OSL decay, the exponents were found more sensitive as compared to amplitudes. This means that the initial guess for the decay parameters have to be given carefully to ensure the convergence of algorithm. A methodology is proposed whereby the exponents are treated as constants in the model. It was found that with this modification it was possible to retrieve the amplitudes from the OSL profiles whose intensity was as low as 500 units. Comparison of CSA and conventional SAR indicated that SAR ages were in general higher. CSA is relevant for heterogeneously bleached sample and in cases where medium and slow components dominate the OSL decay. Besides this, CSA could help isolate fast component of the Quartz signal from a feldspar contaminated sample.

- The CSA has been successfully helped elucidate bleaching status of tsunami sediment. The conventional SAR analysis of nine Tsunami sand had a paleodose ranging from 0.5 to 0.7Gy while the CSA consistently showed the paleodose of ~0.2 Gy. this suggested that the Tsunami picked up sediments from the inter-tidal region and tsunami duration was enough to cause complete bleaching of sediments.. This paleodose distribution using CSA along with bathymetry and attenuation of light under water made it possible to estimate the amount of sediment transported by the Tsunami.
- Paleodose estimation of sediments relies on the experimental parameters. In view of this, the cross-talk was estimated for the TL-OSL readers used in present studies. The OSL measurement protocols were so modified that the distinctive measurement of both irradiation and illumination cross-talks could be made possible. These studies suggest that TL-OSL reader had an irradiation cross-talk of about 3-4% and that the illumination cross-talk could deplete the signal of the adjacent disk by 40-50%. All measurements were done to ensure that samples were placed in a manner that minimizes the cross-talk.

6.2 Future outlook

The present study on quartz suggests that in general OSL of Quartz can be described by a sum of three exponentials. It is also established that the 325 °C TL peak and OSL signal are in general correlated. It would therefore be of interest to examine the relative contribution of individual OSL components to TL. Such correlation studies are extremely important from the view point that they have wide implications for the dosimetric protocols using OSL signal. In this context covariance mapping offers itself as an excellent tool to quantify the correlation between the OSL components and the glow peaks. Covariance signifies the deviation in two distinct measurements of two distinct experimental quantities. This necessitates the existence of an experimental parameter which would affect both glow curve and the OSL signal. In view of this, it is proposed that the dosed sample be optically bleached for varied times and the possible correlation between TL and OSL components be studied by examining the covariance between the area underneath the TL profile and OSL components. It is expected that, the covariance analysis would provide a quantitative measure of the linkage between two different variables namely TL profile and OSL component.

The complete resetting of the luminescen

components. Of late, the wavelet analysis has become an important tool in signal processing. It has been shown that with an appropriate wavelet, SNR of a noisy signal can be drastically improved. In view it is proposed that the wavelet analysis be used to remove the noise from the single grain OSL signal and subsequently the processed signal be used for component specific analysis.

Alanine (α -Amino propionic acid) with the molecular formula $\text{CH}_3\text{CH}(\text{NH}_2)\text{COOH}$ was the first amino acid prepared by chemical synthesis. The elemental composition, electron density, effective atomic number ($Z_{\text{eff}}=6.2$) and density (1.4g/cm^3) are close to that of soft biological tissue. Its tissue equivalence, the radiation sensitivity and stability of radiation induced paramagnetic radicals produced made it a favored candidate for EPR dosimetry for radiation therapy. Further, an Extensive EPR work on the radiation effects in alanine has established the existence of three stable radicals R1, R2 and R3. Thus the OSL study of alanine would provide an ideal ground to test the caveats developed thus far for component specific analysis of OSL from Quartz. Besides this, such study would also help establish the dosimetric properties of Alanine and the universality of the LET effect reported by Mckveer in context of Al_2O_3 .

The carbon nanotube finds an extensive application owing to its remarkable mechanical, electronic, magnetic, photonic, and transport properties. The unique structure allows it to act as a host lattice for intercalation and storage of atoms or molecules. Further, the carbon nanotube has large aspect ratio and it can be treated as ideal one-dimensional systems. These fascinating properties of the carbon nanotube have initiated a feverish activity in the field of nanotechnology. All the applications mentioned thus far are intimately related to the unique structure of the nanotube and it become imperative to study the stability of the nanotube against any structural distortion and defects that may occur during its manufacturing. The quenching of photoluminescence of the nanotube is often attributed to non-radiative decay mechanism due to the presence of defects on the nanotube. In laboratory experiments the structural defects could be created by bombarding the nanotube with electron beam. Thus, the study of luminescence from the nanotube offers the possibility to investigate the structural defects on the

nanotube. Scant studies are available in this regard and it would be worth while to investigate the correlation between the luminescence from the carbon nanotube and its structural distortion. Besides this, such studies would allow one to gain insight into the exact mechanisms leading to the luminescence from the nanotube.

Appendix

Nonlinear least squares fit

The problem of fitting a model i.e. mathematical function to experimental data essentially involves determination of parameters of the function so that the deviation of the experimental data from that predicted by model function is small. The method of least squares can be considered as a special case of a more generalized method of maximum likelihood.

Principle of maximum likelihood

Assume that the experimental data consists of an ordered pairs (x_i, y_i) where y_i is dependent variable and x_i is independent variable. Let the model function which depends on the parameters a and b be represented by $f(a, b; x)$. Further, assume that the measured value y_i is itself drawn from a Gaussian distribution with mean $f(a, b; x_i)$ and standard deviation σ_i [1]. Hence the probability that a measurement results into value y_i is thus given by

$$P_i = \frac{1}{\sigma_i \sqrt{2\pi}} \exp \left[-\frac{1}{2} \frac{(y_i - f(x_i))^2}{\sigma_i^2} \right]$$

Where σ_i is standard deviation for the observations about the value $f(x_i)$. The probability (P) for getting a set of measurements consisting of the N values of y_i is the product of the probabilities for each observation P_i . Thus,

$$P(a,b) = \prod_{i=1}^N P_i = \prod_{i=1}^N \frac{1}{\sigma_i \sqrt{2\pi}} \exp -\frac{1}{2} \frac{y_i - f(x_i)}{\sigma_i}^2 \quad (2)$$

Thus, the maximum likelihood estimates for parameter a and b are those values that maximize the probability P. As evident from equation (2), the probability P is independent of parameters a and b and maximizing P is equivalent to minimizing the sum in the exponential. This sum in the exponential is known as goodness-of-fit parameter and is denoted by χ^2 i.e.

$$\chi^2 \equiv \sum_{i=1}^N \frac{y_i - f(x_i)}{\sigma_i}^2 \quad (3)$$

Thus, the method for finding the optimum fit to the data is equivalent to find the value of a and b that minimize this weighted sum of squares (“least square”) of the deviations χ^2

$$\frac{\partial \chi^2}{\partial a_j} = \frac{\partial \chi^2}{\partial a_j} \sum_{i=1}^N \frac{y_i - f(x_i)}{\sigma_i} = -2 \sum_{i=1}^N \frac{1}{\sigma_i^2} (y_i - f(x_i)) \frac{\partial f(x_i)}{\partial a_j} = 0 \quad (5)$$

If the above set of equations is linear in all parameters, then the parameters can be retrieved by solving the set of m coupled equation. However, if these equations are nonlinear in any of the parameter, χ^2 must be treated as a continuous function of m parameters. In such a case optimized parameters are obtained by searching m-dimensional parameter space for minimum value of χ^2 .

There are many methods which fall in category of Least Square fit. Taylor Method, Gradient Method, Levenberg–Marquardt Method and powell's Dog Leg Method are a few to name [2-4]. Here Taylor and Gradient methods are concerned with the algorithm used for fitting and they shall be described in detail in subsequent sections.

Taylor method

The Taylor method is similar to the Newton method for finding the roots of a function [5, 6]. In order to keep the clarity in explanation of the method a few mathematical representation used are described below.

(x_i, y_i) : This ordered pair represents the measured experimental data. x_i is an independent variable and y_i is dependent variable. Index i runs from 1 to N where N is number of data point recorded.

$f(x_i; a_1, a_2, \dots, a_m) \equiv f(x_i; \hat{a})$: $f(x_i; \hat{a})$ is the model function to be fitted to data.

This function depends on x_i and m parameters namely a_1, a_2, \dots, a_m . This set of parameters is collectively denoted by vector \hat{a}

$\chi^2(\hat{a}) \equiv \sum_{i=1}^N \frac{y_i - f(x_i; \hat{a})}{\sigma_i}^2$: $\chi^2(\hat{a})$ is the objective function to be minimized.

$H_{ij} \equiv \frac{\partial^2 \chi^2}{\partial a_i \partial a_j}$: H_{ij} are elements of matrix \mathbf{H} . \mathbf{H} is known as Hessian and it shows

the curvature of χ^2 surface near minimum.

$\nabla_a \chi \equiv \frac{\partial \chi}{\partial a_1}, \frac{\partial \chi}{\partial a_2}, \dots, \frac{\partial \chi}{\partial a_m}$: $\nabla_a \chi$ is gradient operator in parameter space

Assume $\chi^2(a)$ to be minimum at $a^0 \equiv (a_1^0, a_2^0, \dots, a_m^0)$. Expanding χ^2 about the vector a^0 that minimize χ^2 we have

$$\chi^2(a^0 + \delta a) = \chi_0^2 + \sum_{j=1}^m \frac{\partial \chi_0^2}{\partial a_j} \delta a_j + \frac{1}{2} \sum_{k=1}^m \sum_{j=1}^m \frac{\partial^2 \chi_0^2}{\partial a_k \partial a_j} \delta a_k \delta a_j \quad (6)$$

Here δa is small increment in vector a^0 and χ_0^2 is the value $\chi^2(a)$ at a^0 . To find the optimum values of parameter equate first derivative of χ^2 with respect to increment δa to zero. Thus,

$$\begin{aligned} \chi^2(a^0 + \delta a) = \chi_0^2 + \sum_{j=1}^m \frac{\partial \chi_0^2}{\partial a_j} \frac{\delta a_j}{\partial(a_k)} + \frac{1}{2} \sum_{k=1}^m \sum_{j=1}^m \frac{\partial^2 \chi_0^2}{\partial a_k \partial a_j} \delta a_j \frac{\delta a_k}{\partial(a_k)} \\ + \frac{1}{2} \sum_{k=1}^m \sum_{j=1}^m \frac{\partial^2 \chi_0^2}{\partial a_k \partial a_j} \delta a_k \frac{\delta a_j}{\partial(a_k)} \quad k = 1, 2, \dots, m \end{aligned} \quad (7)$$

In above equation

$$\frac{\partial \delta a_j}{\partial(\delta a_k)} = \delta_{jk} = \begin{cases} 1, & j = k \\ 0, & j \neq k \end{cases} \quad (8)$$

Using equation (8) equation (7) reduces to

$$\frac{\partial \chi^2}{\partial \delta a_k} = 0 + \frac{\partial \chi^2}{\partial a_k} + \sum_{j=1}^m \frac{\partial^2 \chi^2}{\partial a_k \partial a_j} = 0 \quad k = 1, 2, \dots, m \quad (9)$$

Expressing above equation in matrix notation

$$\hat{\nabla}_a \chi^2 + \mathbf{H} \delta a = 0 \quad (10)$$

i.e.

$$\begin{array}{cccccc} \frac{\partial \chi_0^2}{\partial a_1} & & & & & \\ & H_{11} & H_{12} & 3 & H_{1m} & \delta a_1 & 0 \\ \frac{\partial \chi_0^2}{\partial a_2} & H_{21} & H_{22} & 3 & H_{2m} & \delta a_2 & 0 \\ & 4 & 4 & 6 & 4 & 4 & 4 \\ & & & & & & \\ & H_{m1} & H_{m2} & 3 & H_{mm} & \delta a_m & 0 \\ \frac{\partial \chi_0^2}{\partial a_m} & & & & & & \end{array} + \quad (11)$$

$$\delta a = -\mathbf{H}^{-1} \hat{\nabla}_a \chi^2 \quad (12)$$

In present context $\delta a = a_{new} - a_0$. Thus

$$a_{new} = a_0 - \mathbf{H}^{-1} (\hat{\nabla}_a \chi^2) \quad (13)$$

Where a_0 is initial set of parameters and a_{new} is refined set of parameters that minimize χ^2 . The numerical implementation of this algorithm is summarized in below steps:

1. Choose an appropriate initial guess a_0 .

2. Compute the elements of \mathbf{H} and $\hat{\nabla}_a \chi_0^2$ using method of finite difference.
3. Compute χ_{new} using equation (13).
4. Convergence crite

curvature of χ^2

References

1. Bevington P. R. and Robinson D. K. (2002). "*Data Reduction and Error Analysis for the Physical Sciences*" 3rd ed. McGraw-Hill Education: New York, pp 352.
2. Bunday B. D. (1985). "*Basic optimization methods*" ed. Edward Arnold: London, pp 136.
3. Madsen K., Nielsen H. B., and Tingleff O., *Methods fro non-linear least squares problems*. 2004, Informatics and Mathematical Modelling Technical University of Denmark. pp. 30.
4. Istratov A. A. and Vyvenko O. F. (1999). "Exponential analysis in physical phenomena". *Review of Scientific Instruments* **70**(2): pp 1233-1257.
5. Press W. H., Teukolsky S. A., Vetterling W. T., and Brian B. P. (1992). "*Numerical recipes in C*" 2nd ed. Cambridge University Press: Cambridge, pp 994.
6. Devries P. L. (1994). "